To the Graduate Council :

I am submitting herewith a thesis written by Vineet Kevin Lasrado entitled "Bench Scale Evaluation of Solution-Growth Based Techniques for Manufacturing HTS Wire/Tape." I have examined the final copy of this thesis for form and content and recommend that it be accepted in partial fulfillment of the requirements for the degree of Master of Science, with a major in Chemical Engineering.

Atul C. Sheth, Major Professor

We have read this thesis

and recommend its acceptance:

Accepted for the Council:

Associate Vice Chancellor and

Dean of the Graduate School

BENCH SCALE EVALUATION OF SOLUTION-GROWTH BASED TECHNIQUES FOR MANUFACTURING HTS WIRE/TAPE

A Thesis

Presented for the

Master of Science

Degree

The University of Tennessee, Knoxville

Vineet Kevin Lasrado

December 1998

For my friends and family

ACKNOWLEDGEMENTS

The author gratefully acknowledges the invaluable help and constant guidance from his research advisors, Dr. Atul C. Sheth and Dr. M. Paranthaman. Sincere appreciation is given to Dr. Joel Muehlhauser and Dr. Jim Chapman for the opportunity to work on this project and to Mr. Robert A. Hawsey for the internship at Oak Ridge National Laboratory. Gratitude is expressed to Dr. Roger Painter for being on the thesis committee and taking time to read and correct the manuscript.

Sincere thanks are extended to Marvis White (UTSI), Dr. Amit Singhal (ORNL), Patrick Martin (ORNL), Elliot Specht (ORNL), Sue Babcock and Edward Young (University of Wisconsin, Madison) for assisting in the experimental work.

The author is indebted to his family for their constant support and encouragement. Without them, this work would not have been possible.

ABSTRACT

High Temperature Superconductors (HTS) offer significant potential cost savings because of their negligible resistance to the flow of electric current. Several methods exist to fabricate HTS wire and other HTS products. An evaluation of the state-of-the-art methods was carried out by the University of Tennessee Space Institute (UTSI). Based on the conclusions of the report, it was decided to focus on the solution-growth based methods to prepare the buffer layer(s) and the superconductor layer. In most of the studies spin-coating is used for fabricating these thin films. However, for manufacturing long lengths of HTS wire dip-coating is an easy method to scale-up. Hence the study of fabricating such thin films by dip-coating is required.

In this work, a dip-coating unit to coat substrates was assembled. Spin-coating was used to coat when the solution was very viscous as in the case of the metalorganic decomposition (MOD) route. The epitaxial growth of lanthanum aluminate (buffer layer) on single crystal substrates and textured substrates, and yttrium barium copper oxide (HTS) on single crystal substrates was studied. In particular, the effect of major process parameters on some of these systems is reported in this thesis. For the superconducting films transport property measurements were carried out. Based on the conclusions of this study recommendations are made for further studies.

TABLE OF CONTENTS

1 INTRODUCTION 1

1.1 Background 1
1.2 Statement of the Problem 3
1.3 Objectives and Approach 3

2 BACKGROUND AND LITERATURE REVIEW 6

2.1 High Temperature Superconducting Wire 6
2.1.1 Substrate 6
2.1.2 Buffer Layers 8
2.1.3 High Temperature Superconductors 8
2.1.4 Insulation/Passivation Covering 10
2.2 Concepts for Manufacturing HTS Coated Wires/Tapes 10
2.3 Evaluation of the Competing Schemes for Fabricating HTS Coated Wires/Tapes 10
2.4 Lanthanum Aluminate 17
2.4.1 Crystal Structure 18
2.4.2 Review of Solution Growth Techniques 18
2.5 YBCO 20
2.5.1 Crystal Structure 20
2.5.2 Review of Solution Growth Techniques 21
2.6 Chemistry of Solution Based Growth Methods 24
2.6.1 Sol-Gel Method 24
2.6.2 Metalorganic Decomposition (MOD) Method 26
2.6.3 Advantages of Solution Techniques Over Physical Methods 26
2.7 Coating Methods 27
2.7.1 Dip-Coating 30
2.7.2 Spin-Coating 40
2.8 Material Characterization 43
2.8.1 X-ray Diffraction 43
2.8.2 Film Thickness and Measurement 45
2.9 Transport Properties and Measurement 46
2.9.1 Critical Temperature for Superconductivity(T_c) 46
2.9.2 Critical Current Density (J_c) 47

3 EXPERIMENTAL METHODS 48

3.1 Solution Synthesis of $LaAlO_3$ Precursor Solution/Gel 48

3.2 Solution Synthesis of YBCO 50
3.2.1 Sol-Gel Route 50
3.2.2 MOD Route 51
3.3 Coating Procedure 51
3.3.1 Dip-Coating of $LaAlO_3$ 52
3.3.2 Spin-Coating 54
3.4 Thermal Processing 54
3.4.1 $LaAlO_3$ (LAO) / $SrTiO_3$ (STO) System 55
3.4.2 LAO/Ni System 55
3.4.3 YBCO/STO and YBCO/LAO 56
3.5 XRD Analysis 57
3.6 Transport Property Measurements 59

4 RESULTS AND DISCUSSION 62

4.1 Hydrodynamic Model for Dip-Coating 62
4.1.1 Data for the Hydrodynamic Model 62
4.1.2 Calculation of Film Thickness 63
4.1.3 Solution of the Hydrodynamic Model 63
4.2 X-ray Diffraction Analysis 64
4.3 Influence of Process Parameters on Film Texture for LAO/STO System 68
4.3.1 Effect of Degree of Hydrolysis (Dh) 68
4.3.2 Effect of Withdrawal Velocity (Vw) 79
4.3.3 Effect of Thermal Processing Atmosphere 82
4.3.4 Effect of Thermal Processing Temperature 85
4.3.5 Effect of Thermal Processing Time 88
4.4 Epitaxial Growth of LAO on Ni(200) 91
4.4.1 Effect of Withdrawal Velocity 94
4.5 Epitaxial Growth of YBCO on Single Crystal Substrates 97
4.5.1 Critical Temperature Measurements 98
4.5.2 Critical Current Density Measurement 104

5 SUMMARY AND CONCLUSIONS 107

5.1 LAO/STO System 107
5.2 LAO/Ni System 108
5.3 YBCO/STO and YBCO/LAO Systems 110

6 RECOMMENDATIONS 111

6.1 YBCO on LAO/STO and LAO/Ni 111
6.2 Combination of Different Methods 111
6.3 Long Length Samples 112

LIST OF REFERENCES 113

APPENDIX - COMPUTER PROGRAM 117

VITA 121

LIST OF TABLES

TABLE		PAGE
2-1	Progress in Raising the Superconductor Transition Temperature (T_c)	9
2-2	List of Published Schemes for Fabricating HTS Films and Wires	11
2-3	List of Parameters for Evaluation of Coated Conductor Manufacturing Schemes	13
3-1	Time-Temperature program for YBCO Processing	57
4-1	Experimental Data for LAO/STO system	75
4-2	Effect of Degree of Hydrolysis on Film Texture for LAO/STO System	77
4-3	Effect of Withdrawal Velocity on Film Texture for LAO/STO System	80
4-4	Effect of Thermal Processing Atmosphere on Film Texture for LAO/STO System	83
4-5	Effect of Thermal Processing Temperature on Film Texture for LAO/STO System	86
4-6	Effect of Thermal Processing Time on Film Texture for LAO/STO System	89
4-7	Effect of Withdrawal Velocity on Texture of LAO/Ni (200) System	95

LIST OF FIGURES

FIGURE		PAGE
1.1	Architecture of HTS Tape	4
1.2	Architecture of HTS Cable	4
2.1	Crystal Structure of Lanthanum Aluminate ($LaAlO_3$)	19
2.2	Crystal Structure of YBCO	21
2.3	Schematic Showing the Film Profile During Dip-Coating	31
2.4	Stages of Spin-Coating	42
3.1	Schematic of Procedure to Prepare the $LaAlO_3$ Precursor Solution, Powder and Film	49
3.2	Schematic of Bench Scale Dip-coating Unit	53
3.3	Time-Temperature Program for YBCO processing	58
3.4	Experimental Arrangement for the Four-Probe Resistivity Determination	60
4.1	Thickness Profile for Full Coated Length of Sample	65
4.2	Film Thickness Profile for Transition Zone	66
4.3	TEM Cross Section of LAO/STO	67
4.4	XRD Theta-2-Theta Scan for LAO/STO Sample (VKLT 01)	69
4.5	Typical Pole Figure for Epitaxial LAO/STO Film (VKLT 01)	70
4.6	Typical ϕ Scan for Epitaxial LAO/STO Film (VKLT 01)	71
4.7	Typical ω Scan For Epitaxial LAO/STO Film (VKLT 01)	72
4.8	Effect of Degree of Hydrolysis on In-Plane and Out-of-Plane Texture	

for LAO/STO System 78

4.9 Effect of Withdrawal Velocity on In-Plane and Out-of-Plane Texture for LAO/STO System 81

4.10 Effect of Thermal Processing Atmosphere on In-Plane and Out-of-Plane Texture for LAO/STO System 84

4.11 Effect of Thermal Processing Temperature on In-Plane and Out-of-Plane Texture for LAO/STO System 87

4.12 Effect of Thermal Processing Time on In-plane and Out-of-Plane Texture for LAO/STO System 90

4.13 XRD Theta-2-Theta Scan for LAO/Ni Film 92

4.14 Pole Figure for LAO/Ni(200) Film 93

4.15 Effect of Withdrawal Velocity on In-plane and Out-of-plane Texture for LAO/Ni System 96

4.16 XRD Theta-2-Theta Scan for YBCO/STO Sol-Gel Sample (VKL 87) 99

4.17 Resistance vs Temperature (K) for YBCO/STO sample by sol-gel route 100

4.18 Resistance vs Temperature (K) for sample MOD 1 (YBCO/STO) 101

4.19 Resistance vs Temperature (K) for MOD 2 (YBCO/LAO) 102

4.20 Resistance vs Temperature (K) for sample MOD 3 (YBCO/STO) 103

4.21 Effect of Magnetic Field on J_c (MOD 3) 106

NOMENCLATURE

a	crystal lattice parameter
g	acceleration due to gravity
H	wet film thickness
H_∞	constant coating wet thickness
J_c	critical current density
O_2	oxygen concentration
p	pressure
q	entrainment per unit width
R	radius of curvature of the wet film
T_∞	dimensionless coating thickness
Ta	thermal processing temperature
T_c	critical temperature
u	withdrawal velocity as a function of distance
U	steady withdrawal velocity
U_i	utility of x_i
U_o	overall utility
Vw	withdrawal velocity
w_i	weight factor for i^{th} attribute
x	distance along the substrate length
x_i	attribute i
X_i	modified attribute i

y	distance along the coating thickness
θ	angle between incident x-ray beam and crystal plane
ω	out-of-plane
ϕ	in-plane
μ	viscosity of the precursor solution
ρ_{TH}	crystalline film density
ρ, ρ_L	density of the precursor solution
σ	surface tension of the precursor solution

Abbreviations

BSCCO	Bismuth Calcium Copper Oxide
CVD	Chemical Vapor Deposition
FWHM	Full Width at Half Maximum
HTS	High Temperature Superconductor
IBAD	Ion Beam Assisted Deposition
LANL	Los Alamos National Laboratory
LAO	Lanthanum Aluminate
LPE	Liquid Phase Epitaxy
MOCVD	Metalorganic Chemical Vapor Deposition
MOD	Metalorganic Decomposition
ORNL	Oak Ridge National Laboratory
RABiTS	Rolling Assisted Biaxially Textured Substrate
STO	Strontium Titanate

TBCCO	Thalium Barium Calcium Copper Oxide
UTSI	University of Tennessee Space Institute
YBCO	Yttrium Barium Copper Oxide

CHAPTER 1

INTRODUCTION

1.1 Background

Superconductivity is the phenomenon wherein a material does not have any resistance to the flow of electricity. A lot of metals, but not all, show modest electrical resistance at ordinary room temperatures, but turn into superconductors when refrigerated near absolute zero. The first metal discovered to be a superconductor was Mercury, soon after the invention (in 1908) of the cryogenic refrigerator that could attain the temperature at which helium becomes a liquid: 4.2 K. In the subsequent 60 years, many more superconductors were found at these very low temperatures. By the 1960s, certain alloys of niobium were made that became superconductors at 10-23 K. It was theoretically believed that there would be no superconductors above 30 K. There would be a lot more applications for superconductivity if it weren't for the very high cost of liquid helium coolant (Sheahen T.P. 1994). The discovery of high temperature superconductors (HTSC) in 1986 by Bednorz and Mueller (Bednorz J.G. *et al.* 1986) led to an unprecedented explosion of research and development efforts world-wide because of the significant potential offered by these materials (Goyal A. *et al.* 1997) . The first superconductor found with critical temperature (T_c) >77 K, and subsequently the most widely studied HTSC, is Yttrium Barium Copper Oxide ($YBa_2Cu_3O_{7-x}$), commonly termed "1-2-3" or YBCO (Sheahen T.P 141). It now became possible to use liquid nitrogen as a refrigerant instead of liquid helium. Since liquid nitrogen is much cheaper than liquid helium, it

became practical to visualize these "High Temperature Superconductors" becoming a commercially viable product. Since superconductors have virtually no resistance to electric current, they offer the possibility of new electric power equipment with improved efficiency, smaller size, and lower operating costs than today's devices (Oak Ridge National Laboratory [ORNL] "High Temperature..." 1). Practical superconducting wires can be broadly classified into 2 main types based on the manufacturing method: (1)Powder-in-tube (First generation wire): The most popular method is called wire-in-tube process. The tube gives shape to the HTSC and strength to withstand the forces during elongation. When the silver tube is subsequently processed into fine wire, the inner core is HTSC (Sheahen T.P. 1994). (2) Coated conductors (Second generation wire): On April 10, 1996, at the spring meeting of the Materials Research Society, ORNL researchers rolled out a new superconductor-a tape 3 mm wide and 15 mm long, and it became a hot item. They announced the development of a process for making the backbone of superconducting wire using a pair of rollers, heat and thin crystalline film. The rolling-assisted biaxially textured substrates (RABiTS) process generated excitement among researchers in the electrical industry because it represented a leap forward in the race to develop fabricable superconducting wire (Krause C. 1996) Buffer layer(s) is/are grown epitaxially on this substrate by various techniques. The word RABiTS may be used to describe just the Ni or the Ni coated with the buffer layer(s). The buffer layer(s) provide(s) a chemical barrier between the superconductor (YBCO) layer and the RABiTS Ni. The superconductor layer is grown epitaxially over the buffer layer(s) to form the second generation HTS tape. The architecture of the HTS tape is shown in

Figure 1.1 and that of the HTS wire in Figure 1.2. The techniques used to grow the buffer layer(s) and superconductor layer are discussed in Chapter 2. The coated conductor can be fabricated by using a combination of the techniques depending on the required final properties of the product.

1.2 Statement of the Problem

Several techniques exist for fabricating coated superconductors at the laboratory scale. The University of Tennessee Space Institute (UTSI) carried out an engineering evaluation of these techniques based on several parameters and ranked them. This report (UTSI 1998) provided the guidelines for the direction of this research. It was decided to focus on the sol-gel method and carry out bench scale experiments to evaluate the same. The ultimate aim is to achieve a coated superconductor carrying a very high critical current density ($J_c > 1$ MA/cm^2 at 77 K). The critical current density of the superconductor is dependant on a number of processing factors which can be broadly categorized as solution, coating and thermal processing parameters.

1.3 Objectives and Approach

The main thrust of this thesis is to study the bench scale dip coating procedure using the sol-gel method for the fabrication of coated superconductors. Spin coating will be considered for viscous solutions if needed. The main system chosen for this study is YBCO/$LaAlO_3$/$SrTiO_3$. The study is divided into two major areas:

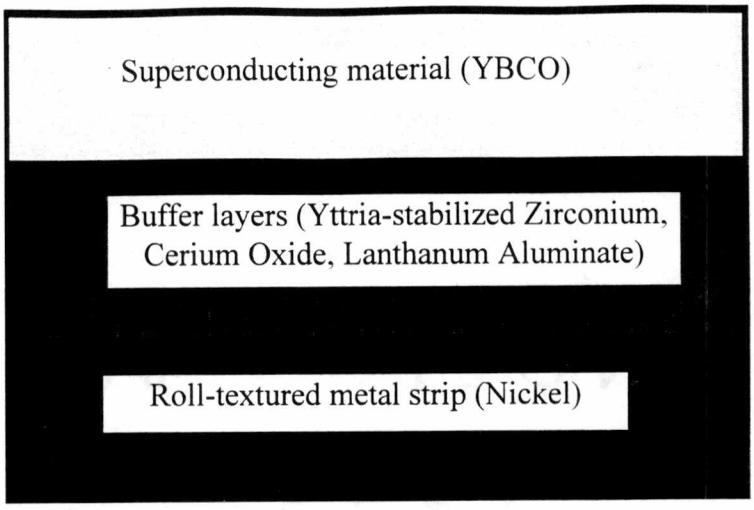


Figure 1.1 : Architecture of HTS Tape

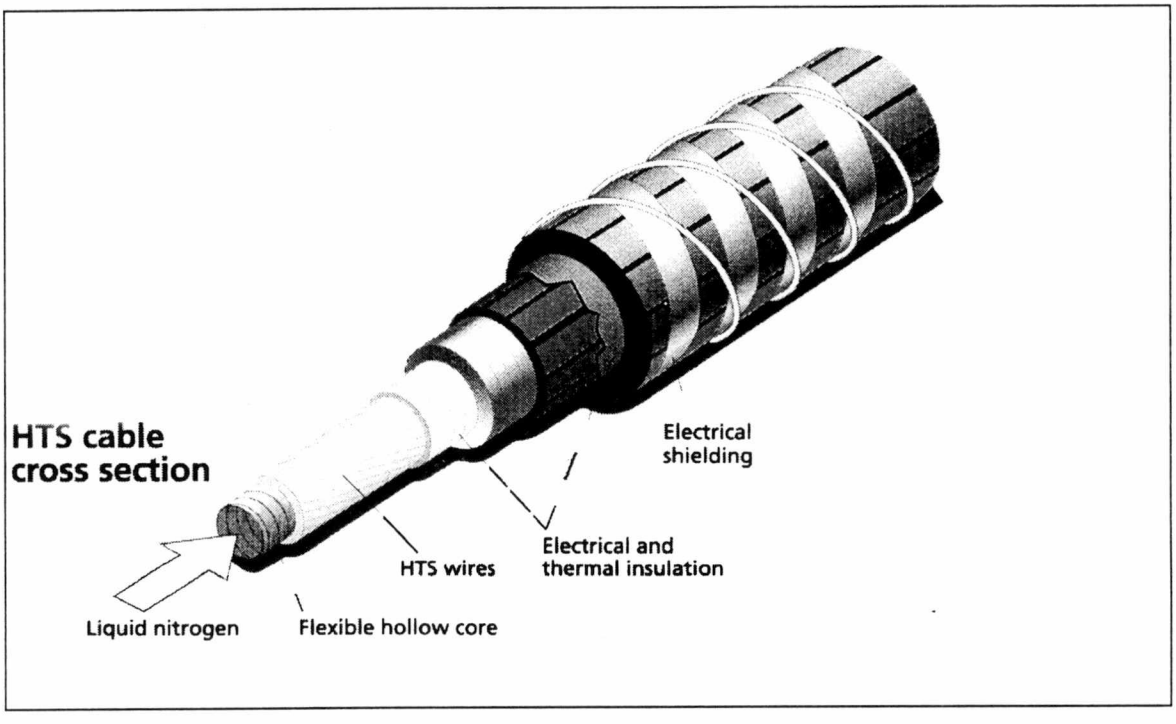


Figure 1.2: Architecture of HTSC Cable (Technology… 1997)

(1) Epitaxial growth of $LaAlO_3$ on $SrTiO_3$(100) and textured metal substrate (RABiTS Ni).

A systematic study of the parameters influencing epitaxial growth of $LaAlO_3$ on $SrTiO_3$ (100) by sol-gel dip-coating will be conducted. Ultimately these buffer layers will have to be grown on textured metal substrates, hence the $LaAlO_3$/Ni(100) system will also be studied. X-ray diffraction will be used to analyze the phase and texture. The texture will then be correlated with the various parameters under study.

(2) Epitaxial growth of YBCO on $LaAlO_3$(100) and $SrTiO_3$(100)

The solution preparation technique for YBCO, unlike that for $LaAlO_3$, has not been well developed. Hence different routes may have to be explored to get the right superconducting phase (Stoichiometry of Y:Ba:Cu =1:2:3) . The focus of this part will be on getting the correct phase with the critical transition temperature T_c in the superconducting range (around 90 K) and a high critical current density ($J_c > 10^5$ MA/cm^2 at 77 K).

CHAPTER 2

BACKGROUND AND LITERATURE REVIEW

2.1 High Temperature Superconducting Wire

The high temperature superconducting wire of the second generation is conceptually thought to be made up of the substrate, buffer layer, HTSC, and the insulation. The following sub-sections describe in detail each of these components.

2.1.1 Substrate

Nickel is the most researched substrate for deposition of buffer layers and high temperature superconductors. There are two existing approaches to use Nickel as a substrate. They are the Ion Beam-Assisted Deposition (IBAD) perfected in 1995 by the Los Alamos National Laboratory (LANL) and the Rolling-Assisted Biaxially Textured Substrates (RABiTS) process developed by ORNL (Krause C. 1996). The IBAD process as the name suggests, uses an ion beam to align the buffer layer with the substrate to achieve in-plane orientation. The RABiTS approach will be explained with more details because substrate prepared by this method was used in this research. This approach involves thermomechanical processing of base metals such as copper or nickel to obtain a very sharp, well developed cube texture. Substrates with biaxially textured, chemically and structurally compatible surfaces for epitaxial growth of superconducting material are referred to as RABiTS. Biaxially textured Ni substrates are formed by consecutive rolling of a polycrystalline, randomly oriented high purity (99.99%) bar to total deformations

greater than 90%. By controlling the surface condition of the work rolls, it is possible to obtain substrates with surfaces as smooth as those obtained by mechanical and chemical polishing. The surface of the substrate can greatly affect epitaxy and integrity of buffer layers and hence critical current density (J_c) of the superconducting film. Obtaining substrates with surfaces adequate for film growth without the need for a cumbersome polishing step is important for scale up to manufacturing of long lengths. Subsequent thermal processing of the substrates in a wide temperature range results in the formation of a sharp cube texture. The texture is stable up to the melting point of Ni (Goyal A. *et al.* 1997). The general approach to grow HTS films with high critical current densities is to achieve epitaxial growth on single crystal substrates. Some of the guidelines for substrate selection are (HTS Wire ... 1996):

- Crystallographic lattice match with the HTS film
- Coefficient of thermal expansion match
- Chemical compatibility
- Thermal stability
- Application specific properties

For example: The superconducting quantum interference device or SQUID requires a rugged combination of substrate and film. In addition to the above criteria the substrate should have low dielectric permittivity and low losses in the frequency of interest (Sheahen T.P 1994).

2.1.2 Buffer Layers

Before coating the high temperature superconductor on the textured metal substrate a buffer layer is required. The role of this layer is to prevent oxidation of the substrate during the thermal processing step or by diffusion of oxygen from the superconductor.

A good buffer layer should have the following properties (Paranthaman M. 1996):

- Smooth and continuous
- Biaxially aligned (Good in-plane and out-of-plane texture i.e. Full Width at Half Maximum (FWHM) $\leq$6-8°)
- Low thermal expansion coefficient mismatch with substrate and superconductors
- Chemically stable up to 780 °C in low partial pressure of O_2, and
- Low lattice mismatch with substrate.

2.1.3 High Temperature Superconductors

After the discovery of high temperature superconductors in 1986, several new superconductors were developed with higher transition temperatures. Table 2-1 enlists some of these superconductors (Owens F.J. *et al.* 1996). While this increase in T_c itself is an amazing result, a high transition temperature is not the only property required to make new compounds useful for applications. As discussed in Chapter 1 there are two main ways of manufacturing a practical superconductor. The powder-in-tube method uses bismuth (BSCCO) or thallium (TBCCO) based materials since they form platelike microstructures after mechanical rolling and drawing (Wu X.D. *et al.* 1995). However BSCCO's performance drops drastically in the presence of magnetic fields. Although

Table 2-1: Progress in Raising the Superconductor Transition Temperature (T_c)

Material	T_c (K)	Year
$Ba_xLa_{5-x}Cu_5O_9$	30-35	1986
$(La_{0.9}Ba_{0.1})_2Cu_4O_{4-x}$ (at 1 GPa)	52	1986
$YBa_2Cu_3O_{7-x}$	95	1987
$Bi_2Sr_2Ca_2Cu_3O_{10}$	110	1988
$Tl_2Ba_2Ca_2Cu_3O_{10}$	125	1988
$Tl_2Ba_2Ca_2Cu_3O_{10}$ (at 7 GPa)	131	1993
$HgBa_2Ca_2Cu_3O_{8+x}$	133	1993
$HgBa_2Ca_2Cu_3O_{8+x}$ (at 30 GPa)	147	1994

YBCO has a lower T_c than BSCCO it can carry high currents even in the presence of magnetic fields over 1 Tesla, making it potentially useful for motors, generators, and other devices that have magnets, such as accelerators and medical diagnostic machines (Kruase C. 1996). Hence there is considerable interest in YBCO superconductor.

2.1.4 Insulation/Passivation Covering

The bare superconducting wire needs to be insulated to so that it can be used as a current carrying cable. Although it seems like this may not be an issue, it is likely that the drop in overall engineering current density and other issues discussed in the evaluation of processes will be important factors in making the right choice(s) for the insulation. Another reason for the insulation is the instability of the YBCO layer when exposed to air and moisture. If the superconductor is not protected from the atmosphere the superconducting properties will deteriorate over time and render the wire unsuitable for use.

2.2 Concepts for Manufacturing HTS Coated Wires/Tapes

The published literature on various schemes to fabricate HTS films on metallic, semi-metallic or ceramic substrates can be divided into physical methods and non-physical or chemical methods. Table 2-2 shows the classification of manufacturing methods.

Table 2-2: List of Published Schemes for Fabricating HTS Films and Wires

Physical methods	Chemical methods
• Sputter Deposition -Magnetron Sputtering (RF and DC) -Ion Beam Sputtering (RF and DC) • Electron beam evaporation • Flash Evaporation • Plasma Spray • Molecular Beam Epitaxy • Laser Ablation	• Chemical Vapor Deposition (CVD) - Metal Organic CVD (MOCVD) -Plasma or Photo Assisted CVD • Sol-Gel Method • Metalorganic Decomposition (MOD) • Electrodeposition • Aerosol/Spray Pyrolysis • Liquid Phase Epitaxy (LPE) • Powder Suspensions or Slurries related -Electrophoresis

2.3 Evaluation of the Competing Schemes for Fabricating HTS Coated Wires/Tapes

To address the potential scale-up issues for the most promising options, one needs to evaluate all of the candidate options first based on some selected parameters. Table 2-3 lists such important parameters. A statistical technique called Multi-attribute analysis was applied to quantitatively evaluate the different methods based on available information for some of the important parameters. Multi-attribute analysis involves the use of an importance rating and a utility rating scheme to determine the best of several alternatives. An additive utility model was used for this analysis, in which the particular option's overall merit/utility U_0, for any combinations of outcomes for n selected attributes(x_1,x_2.....x_n) can be expressed as:

$$U_0 = \sum_{i=1}^{n} w_i U_i(x_i)$$

where :

w_i = weight (scaling) factor for i^{th} attribute, and

U_i = utility of the outcome x_i was specified such that for each attribute x_i, $U_i(x_i = x_i^l) = 0$ and $U_i(x_i = x_i^h) = 1.0$. The shape of the utility function was constructed to give more emphasis to the regions closer to the worst and best cases. This function can be chosen as:

$$U_i(x_i) = 1 - \sqrt{(1 - X_i)^2} \quad \text{where } X_i = \frac{x_i - x_i^l}{x_i^h - x_i^l}$$

Table 2-3: List of Parameters for Evaluation of Coated Conductor Manufacturing Schemes

Substrate	**Buffer Layer**	**Superconductor**	**Passivation/ Insulation**
Materials related parameters			
Compatibility	Compatibility	Compatibility	Compatibility
Mechanical Properties	Availability	Precursor Availability	Availability
Availability	Thermal Expansion	Chemical Stability	Mechanical Properties
Cost	Chemical Stability	Cost	Cost
Thermal Expansion	Lattice Mismatch	Thermal Expansion	Thermal Expansion
Magnetic Properties	Cost	Lattice Mismatch	Oxidation Resistance
	Diffusion Barrier	Diffusion Barrier	Electrical Properties
	Oxidation Resistance		
Pretreatment Related			
Rolling Characteristics	Smoothness	Film Surface Quality	Smoothness
Texture/Orientation	Biaxially aligned	Deposition Rate	Coating Thickness

Table 2-3 continued

Substrate	**Buffer Layer**	**Superconductor**	**Passivation/ Insulation**
Thermal Processing	Continuous/Semi-Continuous	Coating Thickness	Continuous/Semi-Continuous
		Texture/Orientation	
Surface Roughness	Biaxially aligned Deposition Rate	Continuous/Semi-Continuous	Reduction in Jc
Grain Boundary Characteristics	Coating Thickness	Film Stoichiometry	
	Material Utilization	Achievable J_c, J_e	
		Material Utilization	
Engineering and Environmental Based Process Parameters			
Process Severity	Process Severity	Process Severity	Process Severity
Process Complexity	Process Complexity	Process Complexity	Process Complexity
Energy Needs	Energy Needs	Energy Needs	Energy Needs
Controllability	Controllability	Controllability	Controllability
Automation	Automation	Automation	Automation
Reproducibility	Reproducibility	Reproducibility	Reproducibility
Cost	Cost	Cost	Cost
Waste Management	Waste Management	Waste Management	Waste Management
Scale-up Potential	Scale-up Potential	Scale-up Potential	Scale-up Potential

If $U_i = 1.0$ turns out to be the least preferred utility/merit then the function can be redefined as:

$$U_i(x_i) = \sqrt{(1 - X_i)^2}$$

This method was successfully used in the past at the University of Tennessee Space Institute (UTSI) in selecting the best anion-exchange resin for desulfurization/dechlorination application out of various candidate resins based on each resin's performance regarding equilibrium capacity, cycle efficiency, solution concentration and cost of resin. In UTSI's study for the resin evaluation, the overall utility, U_0 calculated using this approach was adequate in selecting the best resin as well as ranking the others.

This multi-attribute analysis technique was applied to the following parameters for which quantitative information was available in the literature:

- Process Severity (Temperature and Pressure)
- Coating Thickness for HTS material
- Deposition Rate for HTS material
- Toxicity and Health Hazards
- Achieved Maximum J_c value
- Cost of Chemicals and Material Utilization Efficiency

For parameters without adequate quantitative data a subjective evaluation was attempted. A scale of 1 to 5 was used where

1 - Highly favorable/acceptable all the time (very good)

2 - Favorable under certain circumstances (moderately good)

3 - Variable (good or bad)

4 - Unfavorable number of times (mostly bad)

5 - Highly unfavorable/unacceptable all the time (very bad)

Using this scale of 1-5 the following parameters were evaluated:

- Raw Material Availability and Cost
- Chemical Stability
- Continuous/Semi-Continuous Operation
- Film Stoichiometry
- Large Area Coverage
- Film Surface Quality
- Material Utilization Efficiency
- Process Complexity
- Energy Needs
- Controllability
- Automation
- Reproducibility
- Current Status/Development Needed
- Scale-up Potential
- Environmental Acceptability
- Safety
- Waste Management

- Corrosion
- Toxicity and Health Hazards

To come up with the appropriate scores for each of the candidate options for the selected parameters help was solicited from the "experts" working in this field of HTS development. Similarly, related literature was also reviewed. External input on the subjective evaluation was received only from ORNL. An in-house subjective evaluation was also prepared at UTSI. A composite score combining both the evaluations was developed. The merit values calculated from quantitative data and subjective evaluation were combined using weighting factors and then further analyzed during sensitivity analysis.

Based on this entire analysis, the MOD and sol-gel are found to be the two leading options from the solution-growth techniques, and MOCVD and PLD are found to be the leading options not too far behind representing the physical/vapor growth techniques. This entire report is available in a report prepared by UTSI (UTSI 1998)

2.4 Lanthanum Aluminate

Lanthanum Aluminate ($LaAlO_3$) is of particular interest as a buffer layer for high temperature superconductors. Critical current densities exceeding 1 MA/cm^2 have been repeatedly observed from YBCO and other superconductors grown epitaxially on single-crystal substrates of this material by various deposition techniques. The lattice mismatch between $LaAlO_3$ and these superconductors is quite small, and $LaAlO_3$ also offers

excellent chemical stability and is possibly an excellent diffusion barrier (Shoup S.S. *et al.* 1997).

2.4.1 Crystal Structure

The crystal structure of $LaAlO_3$ is shown in Figure 2.1 . Earlier studies were carried out to verify the crystal structure of $LaAlO_3$ prepared by the sol-gel route. The cubic lattice parameter of well-crystallized $LaAlO_3$ crystal with $a = 3.796$ Å agreed well with the literature value. At room temperature $LaAlO_3$ has a hexagonal structure which transforms to cubic above 435 ± 25°C. Initially researchers concentrated on the elucidation of catalytic properties of this compound towards the hydrogenation and hydrogenolysis of hydrocarbons (Peshev P. *et al.* 1994).

2.4.2 Review of Solution Growth Techniques

Films of $LaAlO_3$ have been previously grown via a sol-gel technique on silicon and sapphire single crystal substrates. The chemistry employed in that work is different from the chemistry used in this work in that, while starting from alkoxides, a chelating agent, acetylacetone, was used to obtain solutions for coating. Fairly complex heat treatments were used but epitaxial growth was not observed (Peshev P. *et al.* 1994). Instead an all alkoxide system based on methoxyethoxide complexes in 2-methoxyethanol has been used in this work. This chemistry has been used with success in preparing lead-based ferroelectric film and epitaxial growth of lead niobium zirconium titanate (PNZT) on

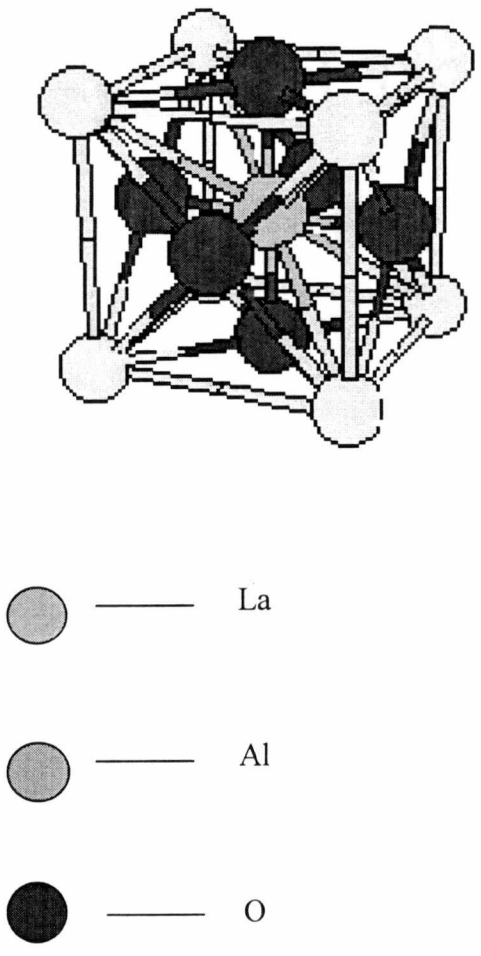


Figure 2.1: Crystal Structure of Lanthanum Aluminate ($LaAlO_3$)

sapphire (Budd K.D. *et al.* 1985). The only other published work on growth of $LaAlO_3$ from solutions is the all alkoxide sol-gel method (Shoup S.S. *et al.* 1997) used in this thesis and the solution preparation steps will be discussed in detail in Chapter 3.

2.5 YBCO

YBCO is the choice HTS material for most coated conductor applications as mentioned earlier. An understanding of the crystal structure of YBCO is necessary to follow the processing of the precursor that yields the crystalline phase.

2.5.1 Crystal Structure

The structure of YBCO is shown in Figure 2.2. It is related to the perovskite structure as follows: by tripling the perovskite (ABO_3 where A and B are elements from the periodic table, usually from the rare elements family in this case) unit cell and substituting one ytrrium atom for every third barium atom, the formula $Y_1Ba_2Cu_3O_9$ results. However, a little more than two oxygen vacancies are required for superconductivity. The formula can be thought of as $Y_1Ba_2Cu_3O_{9-2-x}$. The unit cell is orthorhombic-almost but not quite three cubes stacked upon one another. A key feature of this unit cell is the presence of two layers or planes of CuO_2. There is widespread agreement that the superconductivity takes place in the CuO_2 planes. The role of yttrium is very minor: it just pries the two CuO_2 layers apart. When yttrium is replaced by many of the lanthanide series, there is no appreciable change in the superconducting properties. Thus, the yttrium (or other choice) serves only as a spacer-a "shim" between two CuO_2 layers. Outside this sandwich (but

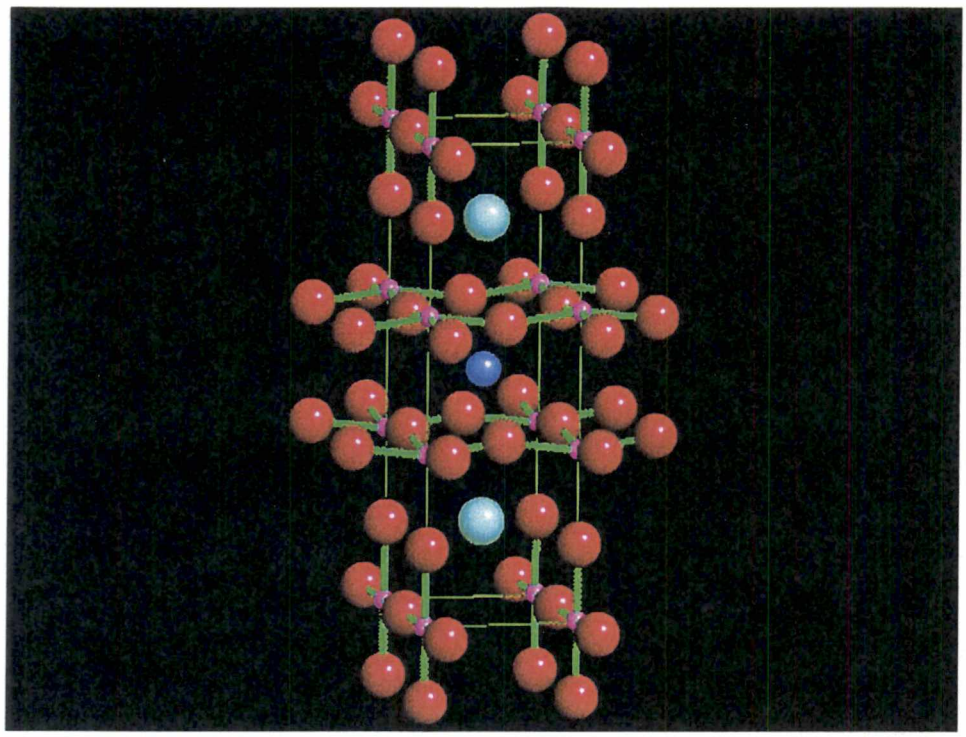


Figure 2.2: Crystal Structure of YBCO

still within the unit cell) is a BaO plane. This means there is one barium atom surrounded by four oxygens along the edges of the unit cell. Finally, at the top (or bottom) of each unit cell is a copper oxide region that has certain oxygen atoms missing. Since this does not qualify as a CuO_2 plane, it is known as a copper oxide chain. Figure 2.2 shows the single yttrium atom and the two barium atoms; the copper oxide planes near the middle contributing one net copper atom (their four copper atoms are shared with the four adjacent unit cells), and the top and bottom chains contribute ½ copper atom (four copper atoms shared with eight unit cells). Hence the name "1-2-3" is also used to refer to YBCO (Sheahen T.P 1994).

2.5.2 Review of Solution Growth Techniques

The most commonly used solution techniques to prepare YBCO precursors may be grouped into three categories:

1. Sol-gel processes that has 2-methoxyethanol as a reactant and solvent. This method works for $LaAlO_3$, $BaZrO_3$, and other such ceramics. Thin films of $Ba_2Ca_2Cu_3O_7$, a precursor of $TlBa_2Ca_2Cu_3O_{9-x}$ (another HTS) have been prepared by sol-gel synthesis from an all alkoxide solution. The J_c reported for this work was 1.9×10^4 A/cm^2 at 77 K (Paranthaman M. *et al.* 1995). Although this technique has been applied with some success to the high-T_c superconductors, it has not been successful for titanates, niobates and tantalates, primarily due to the lack of a highly soluble, moisture-sensitive copper alkoxide.

2. Hybrid processes that use cheleating agents such as acetylacetonate or diethanolamine to reduce alkoxide reactivity. The most general methods are the amorphous citrate method and the Pechini method. The mechanism of the sol formation for the amorphous citrate method, where hydrocarboxylic acid such as citric acid is used as the chelating agent, is that the COO^- anions, which are formed from the dissociation of the citric acid in water, react with the cations to form sols through ionic binding. In the Pechini method, a mixture of hydrocarboxylic acid (citric acid) and hydroxyl alcohol (ethylene glycol) is used, in which chelated citric acid plays the role of distributing the cations throughout the polymeric hydrocarboxylic acid such as poly(acrylic acid) has been substituted for citric acid (Sun Y. *et al.* 1996)

3. Metalorganic decomposition (MOD) technique that uses high molecular weight precursors, and water insensitive carboxylates, 2-ethylhexanoates, etc. (Singhal A. *et al.* 1998). The metal trifluoroacetate method especially is of interest because it avoids the formation of $BaCO_3$, during decomposition. Instead barium, yttrium and copper trifuoroacetates decompose in oxygen to oxy-fluorides which are later converted to the oxides by reaction in a moist furnace atmosphere. Various articles use this method with variations and report different values of J_c. Films grown on $SrTiO_3(100)$ single crystal substrates and thermally processed at 750°C in a humid, low concentration of oxygen gas mixture followed by slow cooling in oxygen resulted in J_cs higher than 1 MA/cm^2 (McIntyre P.C. *et al.* 1990). An ex-situ process that requires thermal processing in a humid atmosphere resulted in films with J_cs greater than 5 MA/cm^2 (McIntyre P.C *et al.* 1992).

2.6 Chemistry of Solution Based Growth Methods

Sol-gel and Metalorganic Decomposition method are the two solution growth based techniques used in this work. The sol-gel technique is used in this work mainly for growth of $LaAlO_3$. It was also used to grow the YBCO film, but had problems due to instability of the precursor solution. MOD was used only to grow YBCO thin films.

2.6.1 Sol-gel Method

The term "sol-gel" is used to describe a process which includes a transition from a "sol" which has fluid like properties to a "gel" which has semisolid-like or viscoelastic properties. Two general types of sol-gel processes can be distinguished:

(i) colloidal sol-gel, the dispersion and aggregation of colloidal (1-100 nm) particles, and

(ii) polymeric sol-gel, the polymerization of a solution containing metalorganics components (Francis L.H. 1991)

The polymeric sol-gel process was used to prepare $LaAlO_3$ in this thesis and hence will be described in detail. The sol-gel process utilizes inorganic or metalorganic precursors to form metal salt, colloidal or polymerizable sols. In aqueous or organic solvents, the precursors are hydrolyzed and polymerized by condensation reactions to form inorganic polymers composed of M-O-M bonds (where M = Metal ion). Although solution viscosity, solids content and substrate wetting are all considerations in sol preparation for thin film formation, the major requirement is that it should remain stable with respect to precipitation or gelation, allowing uniform deposition by dipping, spinning, etc. When alkoxide precursors are employed for sol preparation, hydrolysis and condensation

reactions leading to M-O-M bond formation dictate the structure of the polymeric species formed in the solution. In the hydrolysis reaction, an alkoxide ligand is replaced with a hydroxyl ligand (Brinker C.J. *et al.* 1996). In particular the reactions with respect to the chemistry of $LaAlO_3$ precursor preparation may be represented as follows:

$La[OCH_2\text{-}(CH_3)_2] + HOCH_2CH_2\text{-}OCH_3 \rightarrow La[OCH_2CH_2\text{-}OCH_3]_3 + HOCH_2\text{-}(CH_3)_2$

$Al(OC_4H_9) + HOCH_2CH_2\text{-}OCH_3 \rightarrow Al[OCH_2CH_2\text{-}OCH_3]_3 + C_4H_9OH$

$La[OCH_2CH_2\text{-}OCH_3]_3 + Al[OCH_2CH_2\text{-}OCH_3]_3 \rightarrow LaAl[OCH_2CH_2\text{-}OCH_3]_6$

The product of the last reaction represents the unhydrolyzed precursor and has a complex structure. Hydrolysis of this solution results in La, Al and O linkages and polymerization. The degree of polymerization depends on the amount of water added and as a result the precursor solution may be partially or fully hydrolyzed. Full hydrolysis generally ends up in gelation and is not used for thin film preparation.

The following reaction represent the series of reactions leading to polymerization during hydrolysis.

Here R = alkyl group

$Al(OR)_3 + H_2O \rightarrow Al(OR)_2OH + ROH$

$La(OR)_3 + H_2O \rightarrow La(OR)_2OH + ROH$

$n\,[Al(OR)_2OH] + n\,[La(OR)_2OH] \rightarrow (\text{---}Al(OR)\text{-}O\text{-}La(OR)\text{-}O\text{----})_n + n[H_2O]$

The last reaction seems to be a very simple reaction but in reality it is a more complex reaction. During hydrolysis, cross linking also takes place in addition to the reactions listed above.

2.6.2 Metalorganic Decomposition (MOD) method

Metalorganic decomposition is a non vacuum method for the preparation of thin films with uniform thickness from liquid precursor solutions. Typically, metal carboxylates dissolved in an organic solvent are deposited onto polished substrates by dip-coating or spin coating. The MOD method differs from the sol-gel method in that the atomic linkages between the atoms like Y, Ba and Cu are not formed in the solution state. Although the precursors of Y, Ba and Cu are miscible they maintain their separate identities until raised to temperatures near crystallization where they start reacting and forming the linkages.

2.6.3 Advantages of Solution Techniques Over Physical Methods

The advantages of solution growth based techniques are listed below:

1. Precise Stoichiometry

The accuracy with which one can prepare multi-component films from solution is limited only by the accuracy of the preparation of the solution and the purity of the starting materials. This is not true of physical methods of film preparation, including laser ablation. It is often difficult to sputter or ablate oxides which contain both heavy and light cations, and as a result preferential sputtering or ablation occurs over the course of a deposition. When evaporating, sputtering or ablating from multiple single-element sources, it is often necessary to make repeated calibration runs.

2. Intimate Mixing

The atomic scale mixing which may be achieved using solution techniques lowers crystallization temperature. The primary reason for requiring high temperatures and long processing times in conventional ceramic processing is due to solid-state diffusion. In multi-cation sol-gel processing, choosing the correct chemistry can put the reactants in intimate contact. This causes the diffusion distances to be exceptionally short, and crystallization can occur easily with the loss of organic solvent material, typically at temperatures between 350 and 800 °C. This is generally several hundreds of degrees below the typical ceramic processing temperatures. In addition, low temperature processing allows the formation and study of metastable phases, and use of thermally sensitive substrates.

3. Separation of Deposition and Crystallization Steps

Depositing at low temperature and then thermally processing at a higher temperature in a subsequent step has a number of advantages. The substrate is not held at a high temperature, so that diffusion of underlying layers does not occur. The films can also be crystallized using rapid thermal processing to further minimize thermal damage to the substrate.

4. Non-Vacuum Technique

For a number of applications, a non-vacuum technique is highly desirable. In the case of the high T_c superconductors, practical conductor development would be greatly facilitated if the buffer and conductor layers could be applied by dip-coating and processed using conventional furnaces in a continuous process (Beach D.B *et al.* 1997)

2.7 Coating Methods

Several methods exist for coating of solutions. The coating processes used industrially can be classified into pre-metered and self-metered coating processes. Most of these coating processes are merely permutations of the sequence of geometric arrangement in which the key task of the coater are performed. These tasks are the distribution of the liquid in the cross-web direction and associated control of the coated film thickness in that direction; the control of the coating thickness in the down-web direction; the deposition of the liquid on the substrate, which includes the displacement of the air previously in contact with the substrate; and the formation of the free surface that bounds the coated film. Pre-metered coating processes are those in which the amount of liquid applied to the web per unit area is predetermined by a fluid metering device upstream, and the remaining task of the coating device is to distribute that amount as uniformly as possible. In slot or extrusion coating, one or several layers of liquid emerge from a coating die in close proximity to the moving web and bridge the gap between the web and die to form a coated film. In slide coating, one of several liquid layers are metered onto an inclined plane to form a falling-film flow that is picked up by the moving web across a narrow gap between the lip at the end of the incline and the web. In curtain coating, the coating die is mounted at a considerable height above the point of coating and the coating liquid(s) fall as an unsupported sheet onto the moving web. The key features that differentiate the three pre-metered coating methods are the length of the liquid bridge that needs to be established between the coating device and the moving substrate; the orientation of gravity with respect to the main direction of flow in the liquid bridge; and

the amount of momentum the coating liquid carries toward the substrate. Resulting from these distinguishing features are the different operating limits and characteristic coating defects. In the self-metered coating processes the final wet film thickness of the coated film is mostly controlled by the interactions of the fluid flow with the coating applicator, rather than the amount of liquid supplied to the coater head as in the pre-metered processes. Dip-coating is the withdrawal of a substrate, either a continuous web or individual pieces of substrate material, from a liquid pool. It is the archetype of the self-metered coating process, since the coated film thickness is controlled entirely by the capillary hydrodynamics involved in the film deposition. Other self-metered processes include knife coating, roll and reverse-role coating. These processes are prototypical of configurations with narrow, rigid metering gaps in which the coating thickness depends mainly on the interplay of viscous forces with the geometry of the coating device and the relative speed of its surfaces. In meniscus roll coating (self-metered), the liquid film arriving at the nip between the rollers is much thinner than the roll separation. In this regime capillarity plays a dominant role. The coated film thickness is not metered by the gap between the rollers, but the process is self-metered in the sense that the film thickness depends on the speed ratio between the rollers, and is influenced by capillarity. Spin-coating does not fall into the above 2 categories but is a specialized process for advanced materials. In this method the liquid is dropped onto a substrate which is then spun at a high speed to achieve uniformly thin films. (Kister S.F. *et al.* 1997). Dip-coating is used to coat $LaAlO_3$ precursor solutions on both single crystal substrates and roll-textured

nickel. The main focus of this thesis is on dip-coating. However spin-coating was employed for coating YBCO.

2.7.1 Dip Coating

Thin films formed by a dip-coating process represent the oldest commercial application of sol-gel technology. The first patent based on this process was issued to Jenaer Glaswerk Schott & Gen in 1939 for silica films (Brinker C.J *et al.* 1994). Dip-coating offers a simple, cost effective method which can be implemented either as a batch or continuous process. Other advantages of dip-coating are its ability to coat large surface areas, complex shapes, and both sides of a plate at the same time. This process has found many applications in both industry and in the laboratory. (Li K.K. *et al.* 1991). In dip-coating the substrate is normally withdrawn from the coating bath at a constant speed U (see Figure 2.3). The moving substrate entrains the liquid in a fluid mechanical boundary layer that splits into two at the free surface. Since the solvent is evaporating and draining , the liquid film has an approximately wedge-like shape that terminates in a well defined drying line. (x=0). When the upward-moving flux becomes balanced by that due to evaporation and draining, the process remains spatially steady with respect to the liquid bath surface. i.e. both the shape and position of the depositing film profile remain steady (Brinker C.J *et al.* 1996).

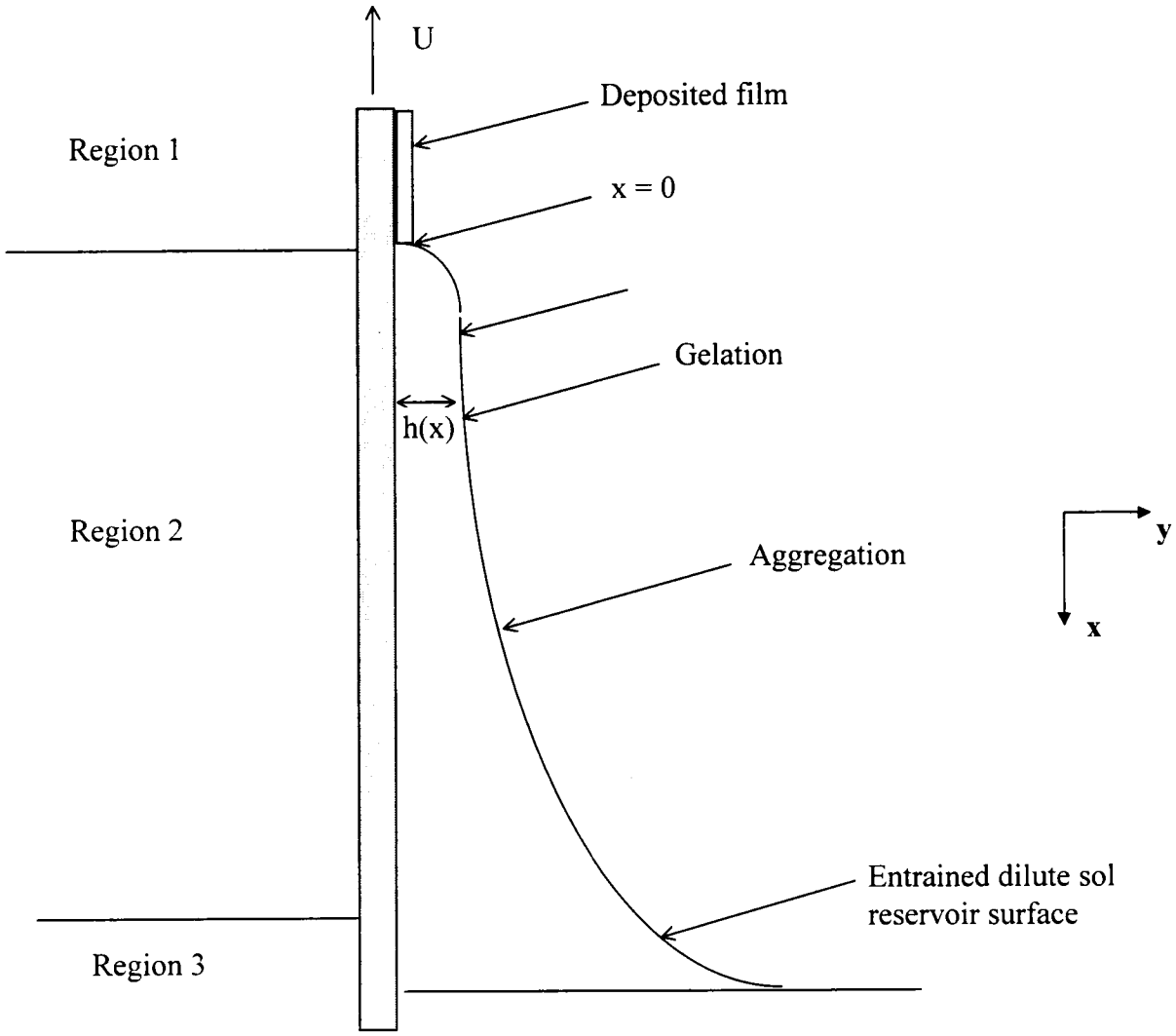


Figure 2.3: Schematic Showing the Film Profile During Dip-Coating

Hydrodynamic model (Middleman S. 1977)

A flat sheet is withdrawn vertically at a speed U from a liquid bath whose free surface is at x=0. Somewhere above the free surface (region 1) a dynamic equilibrium between effect of gravity and the drag of the sheet leads to a constant coating thickness H_∞ . In region 3, nearest the free surface we assume that the effects of surface tension are dominant, in comparison to viscous and gravitational forces. In region 2 the free surface is the result of the interaction among viscous, gravitational, and interfacial forces. In all regions usually inertial effects are neglected.

Region 1

Here, the dynamic equations for a Newtonian liquid reduce to

$$\mu \frac{d^2u}{dy^2} - \rho g = 0 \qquad \text{---(2.1)}$$

where u = substrate velocity, ρ = precursor solution density y= distance in direction of coating thickness and μ = precursor solution viscosity

and the appropriate boundary conditions are

u = U on y = 0 (no slip)

$\mu \frac{d^2u}{dy^2} = 0$ on $y = H_\infty$ (no shear exerted by the air)

u(y) is found to be

$$u = U + \frac{\rho g}{\mu}\left(\frac{y^2}{2} - H_\infty\right) \qquad \text{---(2.2)}$$

Since H_∞ is unknown a priori the solution is not complete. It will be necessary to find u(y) for region 2, and in matching the solutions so that they are continuous between the two regions, an additional condition on H_∞ will appear.

At this stage that the liquid film is not in plug flow; there is a distribution of velocity. Near the web the fluid is moving upward with velocity U. At the surface the fluid has a lower velocity due to the effect of gravity.

Region 2

Here the dynamic equations include pressure (p) and take the form

$$\mu \frac{d^2u}{dy^2} - \rho g - \frac{\partial p}{\partial x} = 0 \qquad \text{---(2.3)}$$

$$-\frac{\partial p}{\partial y} = 0 \qquad \text{---(2.4)}$$

subject to the boundary conditions

On y = 0: u = U (no slip)

On y = H: $\tau \bullet s = 0$ (no shear)

On y = H: $p - \tau \bullet n = \frac{\sigma}{R}$ (continuity of normal stress),

where σ = surface tension of the precursor solution

The two stress boundary conditions are written as shown because the free surface H(x) is not a coordinate surface of the Cartesian system with respect to which u and τ are measured. s and n are unit vectors tangential and normal to the free surface, respectively, and $\tau \bullet s$ and $\tau \bullet n$ are the shear and normal components of stress. In effect the lubrication approximations are introduced here, with the thought that the upward component of

velocity dominating the flow derivatives of u in the y direction is more important than that in the x direction. Thus the flow in this region is taken to be almost parallel to the sheet.

The free surface can be described by the (unknown) function H(x), and the radius of curvature of the free surface R(x) is given by

$$\frac{1}{R(x)} = \frac{-d^2H/dx^2}{\left[1+(dH/dx)^2\right]^{3/2}} \qquad \text{---(2.5)}$$

In region 2 the curvature is taken to be sufficiently small ($|dH/dx| \leq 1$), resulting in the following approximations as boundary conditions:

$\tau \bullet s = \tau_{xy} = 0$

$\tau \bullet n = \tau_{yy} = -\tau_{xx}$

$$\frac{1}{R(x)} = -\frac{d^2H}{dx^2}$$

The boundary conditions reflect the following ideas:

(i) For small $|dH/dx|$ the free surface is nearly vertical, and the shear stress is well approximated by τ_{xy}.

(ii) By the same token $\tau \bullet n$ is approximated by τ_{yy}. Since we appear to neglect a y component of velocity, there is temptation to set $\tau_{yy} = 0$. However, one must note that for a Newtonian fluid in a two-dimensional flow, $\tau_{yy} = -\tau_{xx}$ is a consequence of the continuity equation alone.

Thus a finite normal stress, which may be calculated from equation 2.6 is considered.

$$\tau_{yy} = -2\mu\frac{\partial u}{\partial x} = \tau_{xx} \qquad \text{---(2.6)}$$

The second boundary condition then takes the form

$$p + 2\mu\frac{\partial u}{\partial x} = -\sigma\frac{d^2H}{dx^2} \quad \text{at } y = H(x) \qquad \text{---(2.7)}$$

Equation 2.3 may be integrated twice with respect to y to give the velocity profile as

$$u = U + \frac{\rho g + dp/dx}{\mu}\left(\frac{y^2}{2} - Hy\right) \qquad \text{---(2.8)}$$

which satisfies the no-slip condition at y = 0 and the no shear stress condition at y= H(x).

At this point it is useful to introduce the entrainment q(per unit width), defined as

$$q = \int_0^H u\,dy \qquad \text{---(2.9)}$$

If equation 2.8 is integrated and solved for the pressure gradient it is found that

$$\frac{dp}{dx} = \frac{3\mu}{H^3}\left(UH - q - \frac{\rho g H^3}{3\mu}\right) \qquad \text{---(2.10)}$$

Since H(x) is unknown integration to find p(x) is not possible but is not required.

A differential equation for H(x) can now be derived. Next equation 2.7 is differentiated with respect to x, equation 2.10 is substituted for dp/dx and then equation 2.8 is used to eliminate d^2u/dx^2. The result is

$$0 = \sigma\frac{d^3H}{dx^3} - 3\mu q\frac{d}{dx}\left(\frac{1}{H}\frac{dH}{dx}\right) + \frac{3\mu}{H^3}\left(UH - q - \frac{\rho g H^3}{3\mu}\right) \qquad \text{---(2.11)}$$

Before dealing further within this equation two points need to be noted: It is nonlinear in H, and it contains the unknown constant q. As a matter of convenience the following dimensionless variables and parameters are introduced:

$$L = \frac{H}{H_\infty} \qquad \text{---(2.12)}$$

$$\xi = \frac{x}{H_\infty}\left(\frac{3\mu U}{\sigma}\right)^{1/3} \qquad \text{---(2.13)}$$

the capillary number $Ca = \frac{\mu U}{\sigma}$ ---(2.14)

and a dimensionless equilibrium coating thickness $T_\infty = H_\infty\left(\frac{\rho g}{\mu U}\right)$ ---(2.15)

Equation 2.11 then takes the form

$$\frac{d^3L}{d^3\xi} - (3Ca)^{2/3}\left(1-\frac{T_\infty^2}{3}\right)\frac{d}{d\xi}\left(\frac{1}{L^2}\frac{dL}{d\xi}\right) + \frac{1}{L^3}\left[L - 1 + \frac{1}{3}T_\infty^2(1-L^3)\right] = 0 \qquad \text{---(2.16)}$$

The unknown parameter q has been replaced by H_∞ by making use of the solution in region 1, equation 2.2, from which it follows that

$$q = UH_\infty\left(1-\frac{\rho g H_\infty^2}{3\mu U}\right) \qquad \text{---(2.17)}$$

Thus equation 2.16 contains an unknown parameter T_∞ [see equation 2.15], and it is necessary to have four conditions imposed on the solution to equation 2.16: three boundary conditions for third-order equation and a fourth condition that will give T_∞.

The four conditions are "matching" conditions. The region 2 solution is required to approach the region 1 solution as ξ gets large. In terms of L, region 1 is characterized by

$$L = 1 \qquad \text{---(2.18)}$$

$$\frac{dL}{d\xi} = 0 \qquad \text{---(2.19)}$$

$$\frac{d^2L}{d\xi^2} = 0 \qquad \text{---(2.20)}$$

Equation 2.18 follows directly from the definitions of L and H_∞. Equations 2.19 and 2.20 reflect the fact that the film thickness is uniform and the interface is flat.

The fourth condition must match the curvature of region 2 with region 3. L is set equal to unity in equation 2.16. The vanishing of all derivatives is compatible with the equation. Hence equation 2.16 has a solution which asymptotically approaches the limiting value of $L = 1$.

Region 3

In region 3, it is assumed that the fluid motion has a negligible effect on the shape of the meniscus, so that H(x) is determined by the static balance between gravitational and interfacial forces:

$$\frac{\sigma d^2H/dx^2}{\left[1+(dH/dx)^2\right]^{3/2}} = \rho g x \qquad \text{---(2.21)}$$

It is possible to integrate this equation and find the slope in the form

$$\frac{dH/dx}{\left[1+(dH/dx)^2\right]^{1/2}} = \frac{\rho g x^2}{2\sigma} - 1 \qquad \text{---(2.22)}$$

(The boundary condition $dH/dx \rightarrow -\infty$ at $x = 0$ has been used here.)

In the static case the slope dH/dx vanishes at a height x_∞ above the surface, with x_∞ given by

$$x_\infty = \left(\frac{2\sigma}{\rho g}\right)^{1/2} \qquad \text{---(2.23)}$$

At that point the curvature is given by

$$\left.\frac{d^2H}{dx^2}\right|_{x_\infty} = \left(\frac{2\rho g}{\sigma}\right)^{1/2} \qquad \text{---(2.24)}$$

In terms of dimensionless variables this is

$$\left.\frac{d^2L}{d\xi^2}\right|_{\xi_\infty} = \frac{\sqrt{2}}{3^{2/3}} Ca^{-1/6} T_\infty \qquad \text{---(2.25)}$$

At this point the following situation is arrived at

Region 1. The "solution" is trivial: $L = 1$

Region 2. The solution has proper behavior for $x \rightarrow \infty$

Region 3. The solution has proper behavior for $x \rightarrow 0$, but "turns around" at x_∞.

The key to the problem of matching solutions in region 2 and 3 lies in the behavior of equation 2.16 for small x (large L)

The method of Wilkinson

Wilkinson *et al.* (Middleman S. 1977) corrected the normal stress boundary condition to the form given above as equation 2.7 and linearized some terms to obtain:

$$\frac{d^3L}{d^3\xi} - (3Ca)^{2/3}\left(1 - \frac{T_\infty^2}{3}\right)\frac{d}{d\xi}\left(\frac{1}{L^2}\frac{dL}{d\xi}\right) + (1 - T_\infty^2)\frac{L-1}{L^3} = 0 \qquad \text{---(2.26)}$$

This is the final equation that is solved using MATLAB to give the thickness profile of the $LaAlO_3$ film on the STO single crystal substrate.

To solve for the steady state film thickness the simplified form of the Wilkinson equation by neglecting the effect of gravity is used. This gives

$$\frac{d^3L}{d^3\xi} - \frac{L-1}{L^3} = 0 \qquad \text{---(2.27)}$$

subject to the same boundary conditions

Landau and Levich solve this equation to give

$$T_\infty = 0.944Ca^{1/6}$$

By substituting for T_∞ and Ca the steady state thickness of the film becomes

$$H_\infty = \frac{0.944(\mu U)^{2/3}}{\sigma^{1/6}(\rho g)^{1/2}}$$

Since in this work the thickness of the fired film was of interest and also was the quantity measured, the liquid film thickness needed to be converted to the fired film thickness. Two major assumptions were made for this conversion (Li K.K. *et al.* 1991)

1. The fired film was fully densified; and

2. The interfacial area between the film and the substrate was always constant, meaning that the shrinkage of the film only occurred in the thickness direction.

$$t_{film} = C(\rho_L/\rho_{TH})H_\infty \qquad \text{---(2.31)}$$

where C = Solution loading factor (fraction of $LaAlO_3$ formed from the precursor solution), ρ_{TH} = density of crystalline $LaAlO_3$, and ρ = density of precursor solution.

This resulted in the following equation

$$t_{film} = C\left(\frac{\rho}{\rho_{TH}}\right)\left(\frac{0.944(\mu U)^{2/3}}{(\sigma)^{1/6}(\rho g)^{1/2}}\right) \qquad \text{---}$$

(2.32)

2.7.2 Spin Coating

Spin coating differs from dip-coating in that the thin films are deposited by centrifugal draining and evaporation. Spin coating can be divided into four stages (see Figure 2.4): deposition, spin-up, spin-off, and evaporation (Brinker C.J *et al.* 1990). Although for sol-gel coating, evaporation normally overlaps other stages. An excess of liquid is dispensed on the surface during the deposition stage. In the spin-up stage, the liquid flows radially outward, driven by centrifugal force. In the spin-off stage, excess liquid flows to the perimeter and leaves as droplets. As the film thins, the rate of removal of excess liquid by spin-off slows down, because the thinner the film the greater the resistance to flow, and because the concentration of the nonvolatile components increases, raising the velocity. In the final stage, evaporation takes over as the primary mechanism of thinning. An

advantage of spin-coating is that a film of liquid tends to remain uniform provided that the viscosity is not shear-dependent and does not vary over the substrate. This tendency is due to the balance between the two main forces: centrifugal force, which drives flow radially outward and viscous force (friction), which acts radially inward. The thickness of an initially uniform film during spin-off is described as follows :

$$h(t) = h_o/(1 + 4\rho\omega^2 h_o t/3\mu)^{1/2} \qquad \text{---(2.33)}$$

where h_o is the initial thickness, t is the time, ρ and μ are the density of the solution and ω is the angular velocity. Even films that are not initially uniform tend monotonically toward uniformity, sooner or later following equation 2.33 . By assuming that the spin-off and evaporation stages are sequential, Bornside (Middleman S. 1977) showed that the final thickness h_f scales as follows:

$$h_f \sim \omega^{2/3} \qquad \text{---(2.34)}$$

Equation 2.34 pertains to Newtonian liquids that do not exhibit a shear rate dependence of the viscosity during spin-off stage. If the liquid is shear thinning (often this is the case for aggregating sols), the lower shear rate experienced near the center of the substrate causes the viscosity to be higher there and the film to be thicker. This problem might be avoided by metering the liquid from a radially moving arm during deposition/spin-up stage (Brinker C.J. *et al.* 1996)

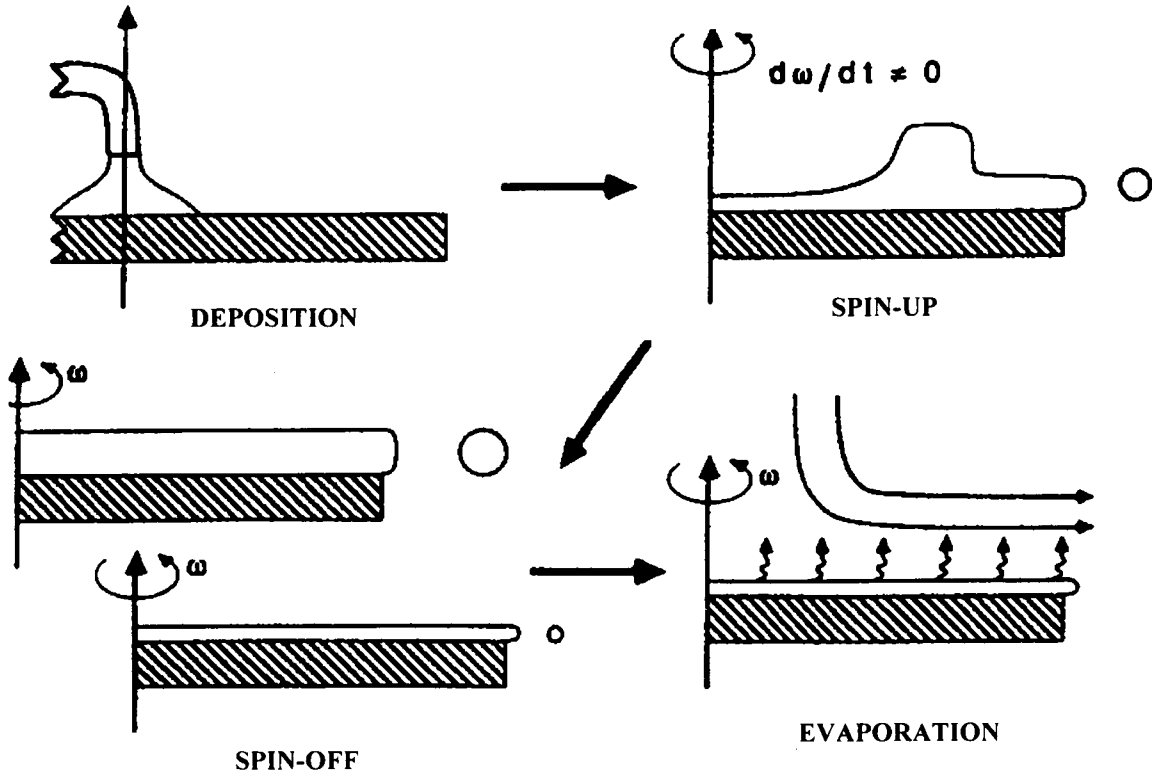


Figure 2.4: Stages of Spin-Coating (Brinker C.J *et al.* 1990)

2.8 Material Characterization

Material characterization is a very broad term that encompasses various aspects related to the testing of a material. In the present study film thickness, epitaxy of the film and transport property measurements of the coatings are the important characteristics.

2.8.1 X-ray Diffraction

The wavelength of x-rays is a few angstroms, which is about equal to the distance between atoms in a crystal lattice. Consequently, x-rays scatter very well off the arrayed atoms in a solid structure. In fact, from a view point of a beam of incoming x-rays, the atoms aligned in their repeating patterns of a crystal lattice appear to be a diffraction grating, and so the outgoing beam of x-rays form a diffraction pattern. In optics, when light enters an interferometer the pattern detected at the output (the interferogram) is related to the spectrum of the incoming light through a Fourier transform. Therefore it is possible to recover the spectrum computationally from a measured interferogram. This is the principle on which most infrared spectrometers work today. It is called Fourier spectroscopy. In an analogous way, a diffraction pattern is related to the Fourier transform of the incoming light and grating. If the incoming beam is monochromatic, then the details of the grating can be recovered by an inverse Fourier transform from the measured diffraction pattern. This technique is used with x-rays to recover information about the crystal structure: starting from the measured x-ray diffraction (XRD) pattern, in principle, a Fourier transform can recover a crystal structure. XRD software can analyze data and match them with the database to identify the phases present. Just as in an optical

diffraction pattern, x-rays interfere destructively except at points where special conditions are met. Imagine a crystal lattice as a series of planes spaced distance d apart, and let the incoming x-rays have wavelength λ. The scattering off one plane will only interfere constructively with that from adjacent planes at those special angles θ (angle between the incident beam and the crystal plane) that meet the Bragg condition:

$$2d \sin\theta = n \lambda$$

A crystal contains parallel planes along three different axes, so the actual measured values of θ vary with the alignment between the crystal planes and the incoming beam of x-rays. A plane perpendicular to the crystallographic a-axis is called the [100] plane; one perpendicular to the b-axis is called [010] plane; and so forth. For complicated crystals like HTSs, there are many choices of planes that contribute to the x-ray diffraction pattern. The custom of plotting 2θ is related to the definition of reciprocal lattice vectors (Sheahen T.P 1994).

The rocking curves are used to find the in-plane and out-of-plane orientations for the coated materials. The width of a rocking curve is a direct measure of the range of orientation present in the irradiated area of the crystal, because each block (subgrain) of a typical mosaic crystal successively comes into reflection position as the crystal is rotated.

Pole figures are used to confirm the epitaxy of the coated material. A pole figure is a stereographic projection, with a specified orientation relative to the specimen, that shows the variation of pole density with pole orientation for a selected set of crystal planes. This

method of describing textures was first used by German metallurgist Wever in 1924, and its meaning can be illustrated by the following example. Suppose one has a very coarse-grained sheet of a cubic metal containing only 10 grains, and that the orientation of each of these 10 grains is to be determined. It is decided to represent the orientations of all these grains together by plotting of their {100} poles on a single stereographic projection, with the projection plane parallel to the sheet surface. Since each grain has three {100} poles, there will be a total of 3 x 10 = 30 poles plotted on the projection. If the grains have a completely random orientation, these poles will be uniformly distributed over the projection. But if preferred orientation is present, the poles will tend to cluster together into certain areas of the projection, leaving other areas virtually unoccupied. The pole figures shown in Chapter 4, represent cube-on-cube texture of the coated material (Cullity B.D. 1978).

2.8.2 Film Thickness and Measurement

The thickness of the grown films is an important process dependant parameter. Several techniques exist to measure the thickness of thin films. They can be classified broadly into destructive and non-destructive techniques. Some of the techniques explored to measure the thickness of the thin films in this work is discussed here. The destructive techniques utilized to determine the thickness of the thin films are Probe Profilometry, Scanning Electron Microscopy (SEM) and Transmission Electron Microscopy (TEM). The Probe Profilometry works on a very simple principle. The sample is placed below the probe and is adjusted so that the moving probe will see both the coated and the uncoated

regions of the sample. This is usually done by leaving a portion of the sample uncoated by masking out a region in between the coated region. However masking of the dip-coating samples may prove to be a problem because of the design restrictions. Thickness between the coated and uncoated parts of the sample does not change suddenly, and that is the probable reason for poor thickness measurement by this method. SEM and TEM are both techniques which involve looking at the interface of the sample and taking a picture. The thickness of the coating can be found by the magnification factor. Sample preparation for TEM is laborious but gives pictures that are superior to the SEM pictures. Some non-destructive techniques were also explored because of the time consuming and tedious nature of SEM and TEM. The non-destructive techniques explored include optical methods which are based on the principles of reflection, absorption and transmission of light. These methods are not well developed for thin sol-gel films (although ellipsometry has been used in the past to determine the thickness of wet and relatively thick films).

2.9 Transport Properties and Measurement

The final performance of the thin films and eventually the superconducting wire depend heavily on the transport properties such as critical temperature (T_c) and critical current density (J_c).

2.9.1 Critical Temperature for Superconductivity (T_c)

A plot of resistance as a function of temperature for superconductors follows a particular pattern. The temperature at which the resistance drops suddenly to near zero is called the critical temperature (T_c) for superconductivity. Resistivity (which is the property of the material and independent of its physical dimensions) of a typical conductor depends linearly on temperature at high temperatures (T) and obeys T^5 Bloch Law (i.e. Resistivity $\propto T^{-5}$) at low temperatures. HTSs have a transition temperature that are in the linear region. Good conductors such as copper and silver have room temperature resistivities of about 1.5 $\mu\Omega$ cm whereas at liquid nitrogen temperatures the resistivity typically decreases by a factor of 3-8. The elemental superconductors, such as Nb, Pb, and Sn, have room temperature resistivities which are a factor of 10 greater than good conductors. The metallic elements Ba, Bi, La, Sr, Tl, and Y, which are also present in oxide superconductors have room temperature resistivities, more than three orders of magnitude greater than that of metallic Cu which puts them within a factor of 3 or 4 of the semiconductor range. The most common way of measuring the resistivity of the sample is the four probe method which is described in Chapter 3.

2.9.2 Critical Current Density (J_c)

Critical current density is the maximum current the superconductor can carry per unit cross sectional area without getting heated. This property is dependant on the properties of the YBCO coating and external parameters such as magnetic field and temperature. The J_c is usually measured at the critical temperature under different magnetic fields.

Chapter 3

Experimental Methods

3.1 Synthesis of $LaAlO_3$ Precursor Solution/Gel

The preparation of the LaAlO3 precursor solution was based on the method used in sol-gel synthesis of $PbTiO_3$ and $PbZrO_3$ (Budd K.D. *et al.* 1985). The weighing of solid materials was done in an argon filled, inert atmosphere glove box, and the solution preparation was carried out under argon using a modified commercial solvent still (Ace Glass). Aluminum sec-butoxide (Alfa,95%), lanthanum isopropoxide (Alfa), and 2-methoxyethanol (Alfa, Spectrophotometric grade) were used without additional purification. The preparation procedure that was followed, including the formation of the powders and films, is schematically described in a flowchart in Figure 3.1.

Aluminum sec-butoxide (1.455 g) was refluxed in 25 ml of 2-methoxyethanol. Approximately 10 ml of sec-butanol/2-methoxyethanol mixture was distilled from the solution which was rediluted with 10 ml of fresh 2-methoxyethanol followed by dissolution. This step was repeated after about 0.5 h. The reaction was carried out at the boiling point of 2-methoxyethanol (124 ° C), for approximately 1.5 h and the exchange of sec-butoxide by methoxyethoxide was presumed finished. The final volume was adjusted to 5ml by distilling out 20 ml of solvent. Lanthanum iso-propoxide (1.9451 g) was refluxed in 25 ml of 2-methoxyethanol. The distilling and redilution was carried out in a manner similar to the aluminum solution. The final volume of the solution obtained was 9ml. The aluminum and lanthanum based solutions were then mixed and reacted for

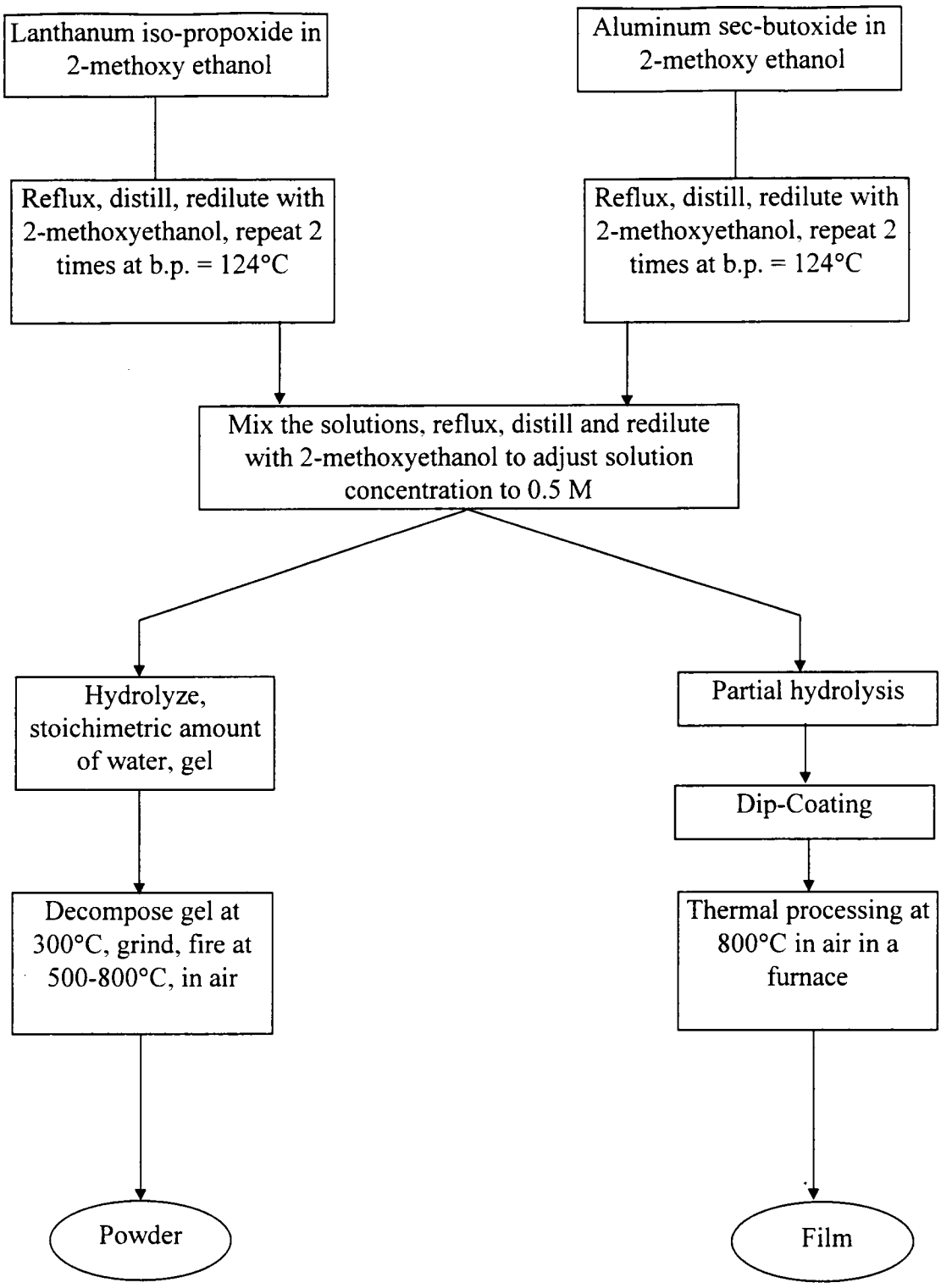


Figure 3.1: Schematic of Procedure to Prepare the $LaAlO_3$ Precursor Solution, Powder and Film

about 0.5 hr at the boiling point (124°C) of 2-methoxyethanol. The final volume of the solution was adjusted to 25 ml. The calculated total cation concentration was 0.22 M. The solutions required for dip-coating were prepared by hydrolyzing this precursor solution with different volumes of 0.22 M water in 2-methoxyethanol. For example: About 8ml of 1:1 solution was prepared by mixing 4 ml of unhydrolyzed precursor with 4 ml of the water in 2-methoxyethanol. The solution was aged for a day before usage.

3.2 Synthesis of YBCO Precursor Solution/Gel

Two different techniques were used to prepare YBCO precursor solution. A sol-gel method involving alkoxides and a metalorganic decomposition (MOD) method starting from 2-ethylhexanoates. The MOD method used here was developed by Dr Amit Singhal at ORNL as a part of the collaborative efforts on this project.

3.2.1 Sol-gel Route

The sol-gel precursor solution was prepared by weighing yttrium isopropoxide (prepared from yttrium metal at ORNL), copper 2-methoxide, and barium metal in the molar ratio of 1:2:3 respectively. Copper 2-methoxide (0.288 g) was dissolved in triethanolamine and stirred overnight in a reaction flask (because the dissolution of copper 2-methoxide in triethanolamine is a very slow process). Yttrium iso-propoxide (0.200 g) was added to a second reaction flask in a dry box the next day and was dissolved in 2-methoxyethanol. Barium metal (0.206 g) was weighed in a third reaction flask , also in the dry box and

similarly dissolved in 2-methoxyethanol (this reaction involves hydrogen formation and hence the gas is allowed to escape to avoid pressure build up in the flask). The yttrium and barium solutions underwent ligand exchange reactions when refluxed separately and charged with fresh solvent. The yttrium and barium solutions were then cooled and mixed and reacted again. Finally the solution was cooled, the copper 2-methoxide in triethanolamine was added and volume of the mixture was adjusted to 25 ml. The final concentration (total cation) of the solution was 0.18 M. This solution was hydrolyzed later to a desired degree using a solution of water in 2-methoxyethanol.

3.2.2 MOD Route

The precursor solution via the MOD route was prepared by mixing yttrium 2-ethylhexanoate (STREM Chemicals, 98.5%), barium neodecanoate (STREM Chemicals, 95%) and copper 2-ethylhexanoate (STREM Chemicals, 98.2%) in a molar ratio of 1:2:3, respectively. The resulting solutions were heated on a hot plate (<100 °C) to prepare a homogeneous solution, but on cooling the solution became very viscous. The prepared solutions do not dip-coat easily because of their high viscosity, hence spin coating was used.

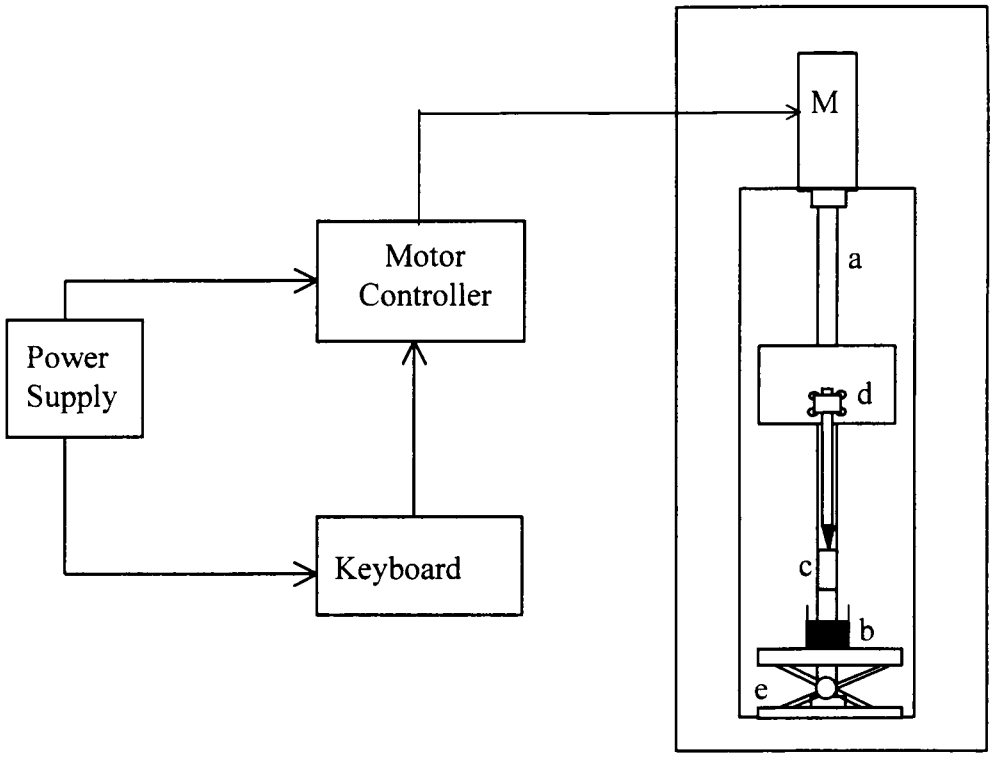
3.3 Coating Procedure

In the HTS research the two most commonly used coating procedures for solution coating are dip-coating and spin coating. Although the main focus of this thesis is dip-coating,

spin-coating was needed to develop YBCO films because of the viscous and unstable nature of the precursor solution prepared following the MOD route.

3.3.1 Dip-Coating of $LaAlO_3$

The $LaAlO_3$ precursor solution was prepared via an all alkoxide sol-gel route starting with aluminum sec-butoxide, lanthanum isopropoxide and 2-methoxyethanol. Different solutions were prepared for coating by varying the degree of hydrolysis for each. Based on previous experiments (carried out at ORNL) involving spin coating and dip coating a set of base conditions was decided. To study the effect of a particular parameter, that parameter was varied while keeping the other parameters at the base conditions. The different parameters under study included degree of hydrolysis of solution, substrate withdrawal velocity, thermal processing temperature, atmosphere and duration. Dip coating was used to coat single crystal substrates of $SrTiO_3$ (100) and textured nickel. The schematic of the dip coating apparatus is shown in Fig 3.2 and it consisted of three major parts: the driving mechanism, solution dispenser and the electronic motor controller. The motor drove a translating unit and arm mounted on a shaft. The motor and drive assembly provided speeds ranging from ~0.03 cm/min to 90 cm/min. The most frequently used speed was 3 cm/min. The substrate was clamped to the translating arm and introduced into the solution until most of the substrate was wetted. The wetted substrate was then withdrawn at a desired speed and allowed to dry while clamped. The high volatility of 2-methoxyethanol did not require any additional drying. The coated substrate was then placed in a ceramic boat. The coated substrate was finally thermally processed in a



a: Shaft

b: Solution dispenser

c: Substrate

d: Translation unit

e: Laboratory jack

Fig 3.2: Schematic of Bench Scale Dip-coating Unit

furnace under varying set of conditions involving different temperatures, atmospheres and times.

3.3.2 Spin Coating

The substrate samples used for spin coating were $SrTiO_3(100)$ or $LaAlO_3(100)$ single crystals (5 x 10 mm size supplied by Commercial Crystal Laboratories, Inc.). They were ultrasonically cleaned in methanol for about 10 minutes and thermally processed in pure oxygen at 800°C. Although this step may not be necessary, it is a common practice to subject the substrates to this procedure so that the substrate surface is clean and any oxygen vacancies in the crystal structure are filled. The pretreatment steps also assist in obtaining superconducting films with superior quality. The pretreated sample was placed on the spinning disc and a vacuum pulled below the sample to ensure that sample was held down. The precursor solution of YBCO was then dropped onto the sample and the sample wetted was manually. The sample was then spun at 4000 rpm for about 40 s.

3.4 Thermal Processing

The dried samples have to be thermally processed for crystallization of the buffer layer and superconductor layer. The procedure varies for each material and can be quite complex especially in the case of YBCO.

3.4.1 $LaAlO_3$ (LAO) / $SrTiO_3$ (STO) System

The dried sample of STO coated with LAO precursor solution was placed in a ceramic boat. A box furnace was pre-heated to 800°C and the sample was placed in the furnace for a desired time ranging from 5-10 minutes. For the systematic study involving different temperatures and processing atmospheres, a tube furnace was used. The furnace was preheated to the required temperature (usually 800°C). The ceramic boat containing the sample was introduced into a quartz glass tube and closed with an end containing quartz tubing for introducing the gas required for processing and allowing for a thermowell. The tube was purged with the gas for about 10 minutes to ensure that the concentration of the gas in the tube is the same as that of the incoming gas. The gases used for thermal treatment ranged from 100% oxygen to different concentrations of oxygen in argon(except 21% oxygen for which air was used) and a mixture of 4% hydrogen in argon. This tube was then inserted into the tube furnace and removed after 5-10 minutes. The quartz glass tube was then allowed to cool down to near room temperature, gas flow was then shut off, and the sample were removed for further analysis.

3.4.2 LAO/Ni System

The samples of LAO/Ni were processed in a similar manner with different process conditions. Oxygen cannot be used as a process gas because nickel will get oxidized at high temperatures. Oxidation causes nickel to lose its texture and is undesirable. Hence an inert atmosphere of 4% hydrogen in argon (called forming gas) was used instead. This

gas was already used in the past with success to grow c-axis oriented films of LAO on textured nickel at ORNL. As a result of the change in atmosphere to reducing conditions the crystallization temperature was raised from near 800°C to around 1150°C. The temperature of 1150°C was used based on the past practice of growing LAO/Ni at ORNL.

3.4.3 YBCO/STO and YBCO/LAO

The thermal processing for YBCO is much more complex than that for $LaAlO_3$. It is a stagewise operation in which the sample is subjected to changes in atmosphere and temperatures. In the present work, the boat containing the coated sample was placed in the quartz tube and pure oxygen gas (100%) was passed through the tube. The tube was purged for 10 minutes to allow concentration of gas in tube to equalize with the incoming gas concentration. The furnace was programmed with the cycle shown in Table 3-1. This cycle was selected based on the past experience for growing YBCO films at ORNL and equilibrium studies of the system (Feenstra R. *et al.* 1991). The graphical representation of this cycle is shown in Figure 3.3. The tube containing the sample was then inserted into the furnace and the program was run. The ramp up rate to 500°C was approximately 2°C/min (slow heating rate allows film to dry without cracking). At around 500°C the gas was changed to 240 ppm oxygen (measured by an oxygen analyzer). The furnace was maintained at this temperature for about 10 min to burn off the carbon. The ramp up rate was then raised to 25°C/min because slow heating was not necessary. The atmosphere was maintained until the furnace temperature reached 820°C and then dropped below

700°C. Once the temperature started falling below 820°C the gas was changed back to pure oxygen. The sample was then left overnight in the furnace while it cooled slowly, and was removed next day for analysis.

3.5 XRD Analysis

The sample was mounted on a sample holder and introduced into the XRD machine. The scan range was entered into the computer controlling the machine (typically 20° -60° for LAO/STO and LAO/Ni and 5°-70° for YBCO/STO or YBCO/LAO). The machine scans the sample and sends the data to the computer. The data is then imported into a library software package for XRD scans (JADE) and analyzed for the expected peaks. The XRD pattern is compared with the expected pattern from the database, which confirms the c-axis orientation (or presence of random phases or orientations, whichever the case). To confirm epitaxy the samples are then analyzed by another XRD analysis which is called the pole figure analysis.

Table 3-1: Time-Temperature Program for YBCO Processing

Time (hr)	Temp (°C)
0	20
4	500
4.2	500
5.2	820
7.7	500
8.7	500
16.7	300
28.7	20

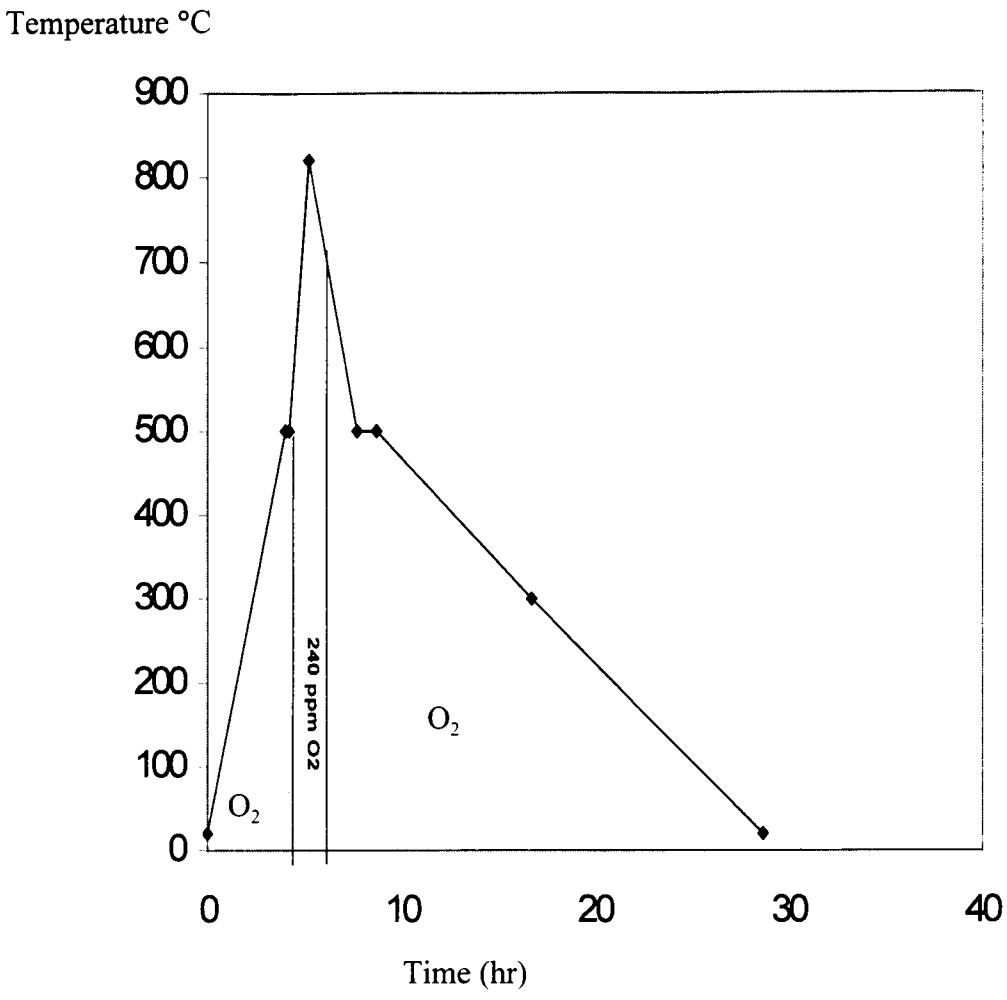


Figure 3.3: Time-Temperature Program for YBCO processing

3.6 Transport Property Measurements

The YBCO sample for which the transport property measurements was carried out had to be prepared for the measurement first. This treatment involved deposition of silver (to make good electrical contact) onto the sample in a specific pattern by sputtering. The sample was then masked with the pattern and coated in a pulse mode (to avoid overheating of the unit) for about one hour after the sputtering unit maintained a stable current of 15 mA after the flow of argon and the voltage were adjusted. The most common way of measuring the resistivity of a sample is the four-probe method sketched in Figure 3.4. This figure shows the basic set-up. The actual measurement procedure is more involved and also includes a cryogenic unit (helium gas) to go as low as 4.2 K if necessary and a data acquisition system connected to a computer. The sample was placed in the unit and proper voltage and current contacts were established. After closing the system, the room temperature resistance was measured and the sample was cooled to about 40 K. The sample was then slowly heated and resistance measured as the temperature increased. The data was read by the computer and the final output printed in the form of a graph from which the T_c value was read. The set-up for J_c was similar with a slight difference. The currents required for T_c measurement were in the 1-200 mA range whereas those for J_c measurement in the 1-20 A range. Hence although the principle of measurement remained the same the experimental set-up required thicker cables to carry these large currents and a liquid nitrogen cooling container sufficed for refrigeration.

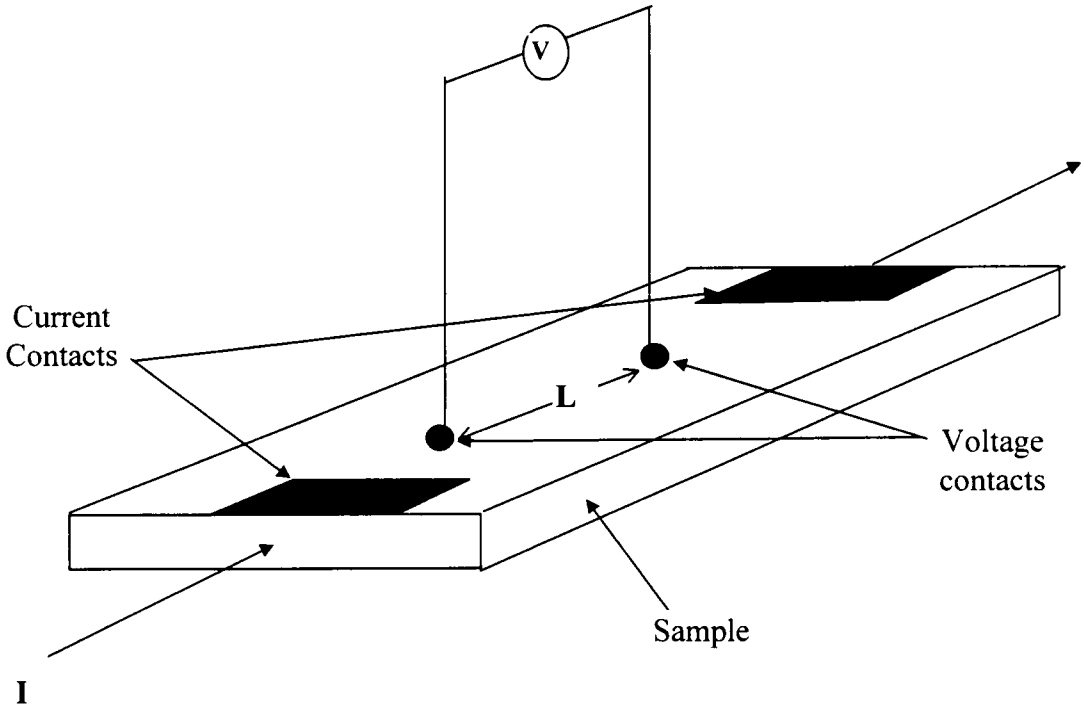


Figure 3.4: Experimental Arrangement for the Four-Probe Resistivity Determination

A magnetic field generation unit was also needed to measure the current densities in the presence of desired magnetic fields.

Chapter 4

Results and Discussion

4.1 Hydrodynamic Model for Dip-Coating

The hydrodynamic model described in Chapter 3 was applied to simulate the of dip-coating of $LaAlO_3$ on $SrTiO_3$ (100) single crystal substrates. The constants needed for the model were measured experimentally or obtained from literature.

4.1.1 Data for the Hydrodynamic Model

The physical properties of $LaAlO_3$ precursor solution are required to test the hydrodynamic model to simulate the dip-coating of $LaAlO_3$ on $SrTiO_3$ (100) substrates. The physical properties required are viscosity, surface tension and density of the solution. These properties were measured at 20°C.

Viscosity μ = 2.5 cps (Brookfield Viscometer)

Surface Tension σ_{LV} = 0.04 N/m (Capillary rise method)

Density ρ = 1541 kg/m^3 (calculated by measuring mass of a certain volume of solution)

Solution Loading Factor (C) = Fraction of $LaAlO_3$ formed from precursor = 0.075

Density of Crystalline $LaAlO_3$ (ρ) = 6500 kg/m^3 (estimated from crystal structure)

Substrate Withdrawal Velocity U = $5*10^{-4}$ cm/s

4.1.2 Calculation of Film Thickness

The film thickness along the substrate length is a function of distance. According to the prediction by the hydrodynamic model the film thickness should become steady after a certain point along the sample. The model was solved using the above parameters to find out this point. The model also gives the film thickness profile as a function of sample length.

Steady state constant film thickness for Newtonian fluid is given by equation 2.32.

$$t_{film} = C\left(\frac{\rho}{\rho_{TH}}\right)\left(\frac{0.94(\mu U)^{2/3}}{(\sigma)^{1/6}(\rho g)^{1/2}}\right) \qquad \text{---(4.1)}$$

Substituting the values for various parameters, gives

$$t_{film} = 0.075\left(\frac{1541}{6500}\right)\left(\frac{0.94\left(0.0025 * 5 * 10^{-4}\right)^{2/3}}{(0.04)^{1/6}(1541 * 9.8)^{1/2}}\right) \qquad \text{---(4.2)}$$

or,

$$t_{film} = 271 \ \text{Å} \qquad \text{---(4.3)}$$

Thus at steady state conditions the constant thickness of the dried film would be about 271 Å.

4.1.3 Solution of the Hydrodynamic Model

The modified hydrodynamic model (non-dimensionlized form of equation 2.16) was solved by using the software package called MATLAB. The stability of the analytical solution usually depends on the length parameter. Since the boundary conditions are unknown for the region of constant thickness, the length parameter has to be long enough to accommodate any variation in thickness. For a small length parameter, the analytical solution represents only the constant thickness region and for large lengths it diverges to unreasonably large thickness. Although it may seem that this should be the other way around, it is not so because the analytical solution begins from the constant thickness region and proceeds towards the lower end of the sample. This hydrodynamic model was solved to give a stable analytical solution and hence an appropriate thickness profile. Figure 4.1 shows the predicted thickness profile for the single crystal substrate, calculated using this model. To verify the model with a high degree of confidence one requires a reliable and feasible technique to measure the actual thickness of several coated samples. For this Profilometry, SEM and TEM were tried to measure the thickness. However Profilometry and SEM posed several problems because the films were extremely thin (1000 $\mathring{A}$ range). TEM was the only technique that was successful for measuring the film thickness. Figure 4.2 shows a picture of the cross section of a sample of LAO/STO taken by TEM. The observed thickness was approximately 1200 $\mathring{A}$. The TEM cross section was taken around the middle of the total coated length. This measured thickness seems to

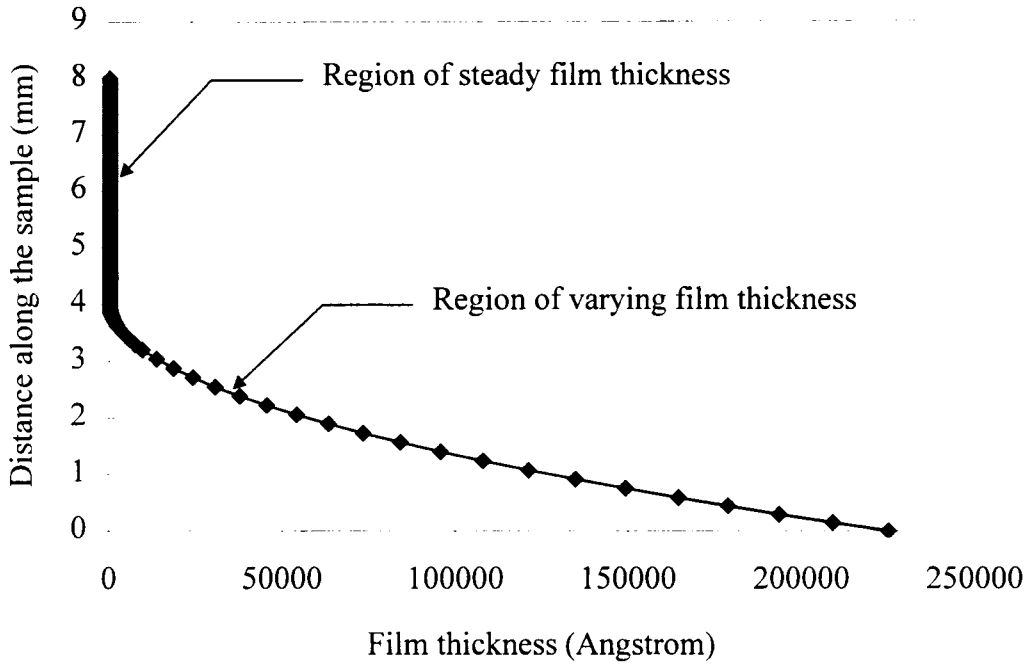


Fig 4.1: Film Thickness Profile for Full Coated Length of Sample

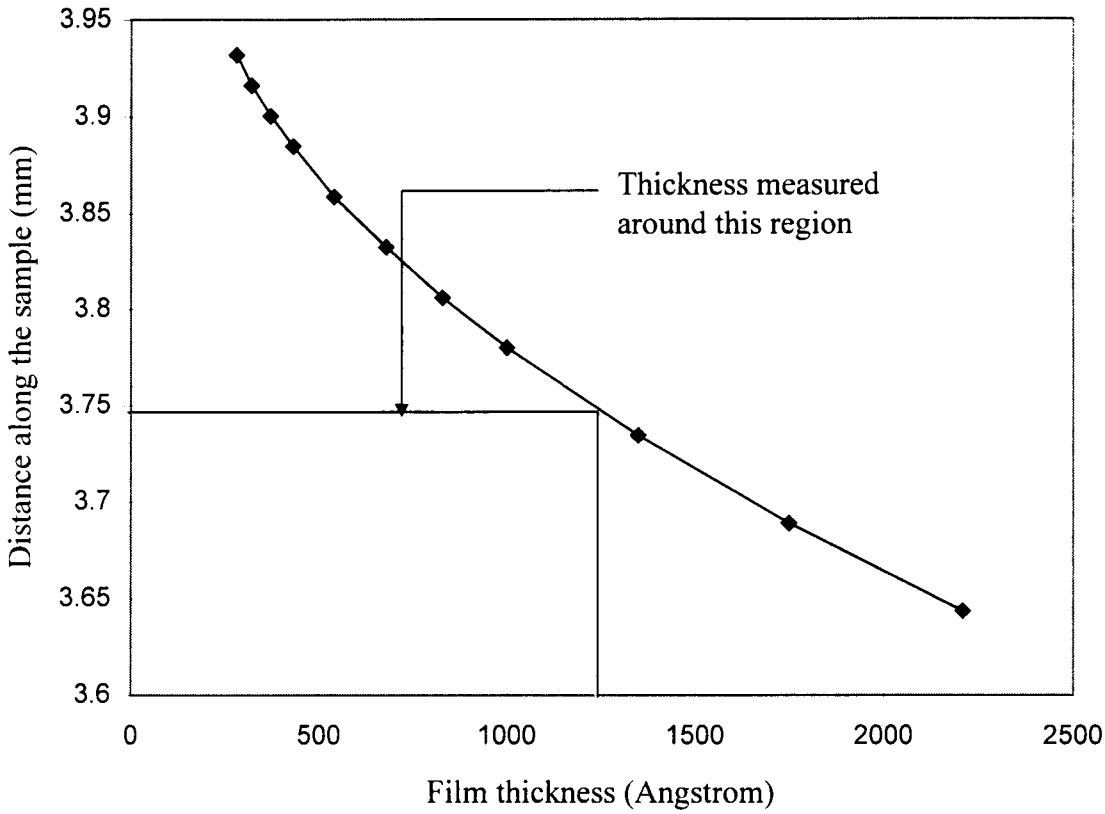


Figure 4.2: Film Thickness Profile for Transition Zone

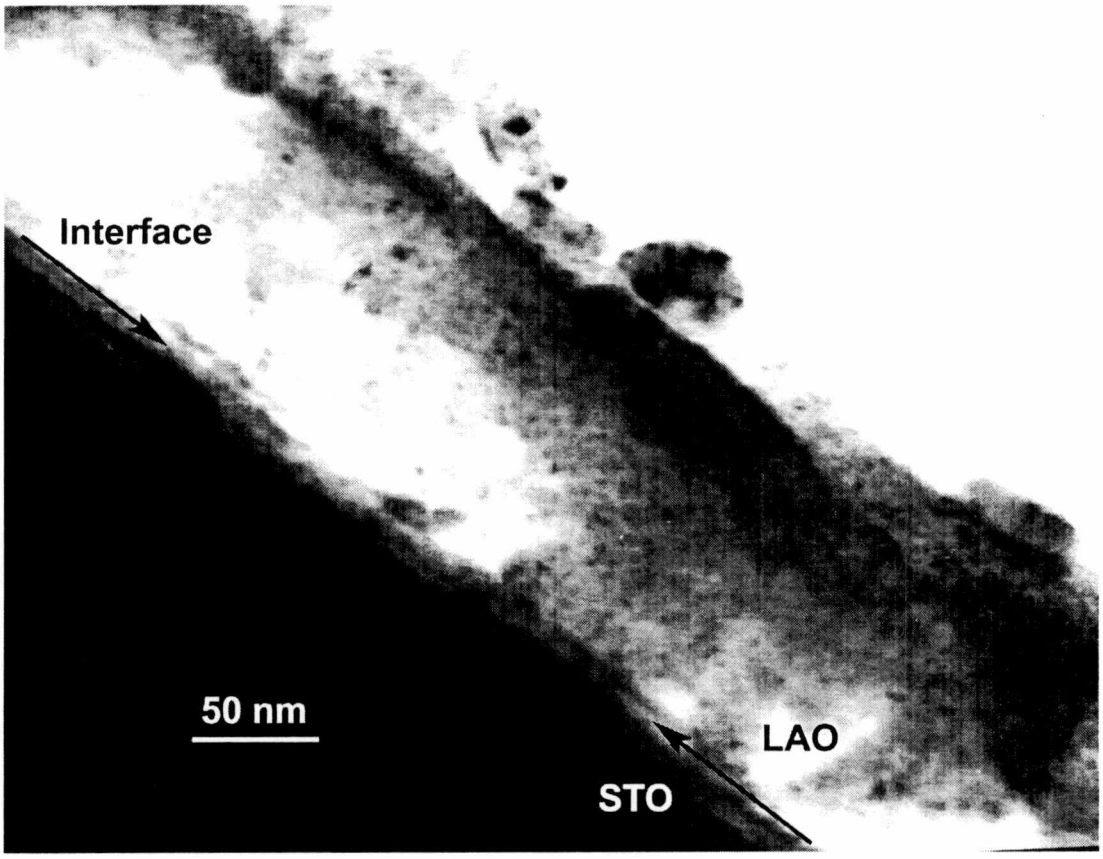


Fig 4.3: TEM Cross Section of LAO/STO

(Courtesy of University of Wisconsin-Madison)

be in agreement with the model predicted thickness near the vicinity of the measurement point.

4.2 X-Ray Diffraction Analysis

Once the samples of LAO/STO were thermally processed, they were ready to be analyzed. The coated samples were scanned by various X-ray Diffraction methods. The 2-theta scan identified the phases present by matching the measured scan with the database using Jade 3.0 (Software package for XRD analysis). A typical 2-theta scan for the LAO/STO system is shown in Figure 4.4. As shown in Figure 4.5, the LAO film exhibited c-axis preferred orientation on a STO(100) single crystal substrate. The LAO peaks were considered to correspond to (001) and (002) planes in a cubic structure. In order to confirm epitaxial growth the pole figure scan is necessary. A typical pole figure scan of the cubic (202) reflections (Figure 4.5) showed a single cube-on-cube epitaxy. A quantitative measure of the growth quality of textured films are usually expressed in terms of the full width at half maximum (FWHM) values for rocking curves obtained by XRD analysis. After the samples are scanned by 2-theta X-ray diffraction for phase analysis they have to be investigated for texture by the rocking curves. The rocking curves were generated by using a Philips X-ray diffraction unit by Marvis White at UTSI. The curves were fitted by appropriate models such as the Gaussian Distribution and Pearson Models. There are two FWHM values, namely ω and ϕ which indicate the out-of-plane and in-plane textures respectively. Typical rocking curves for the LAO/STO system are shown in Figure 4.6 (ϕ scan) and Figure 4.7 (ω scan).

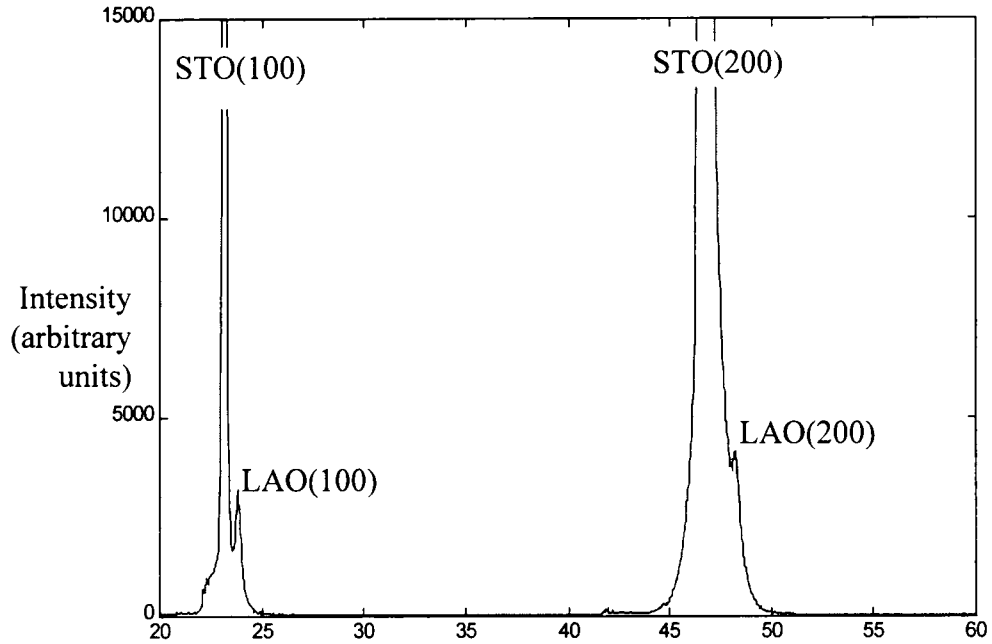


Figure 4.4: XRD 2-Theta Scan for LAO/STO Sample (VKLT 01)

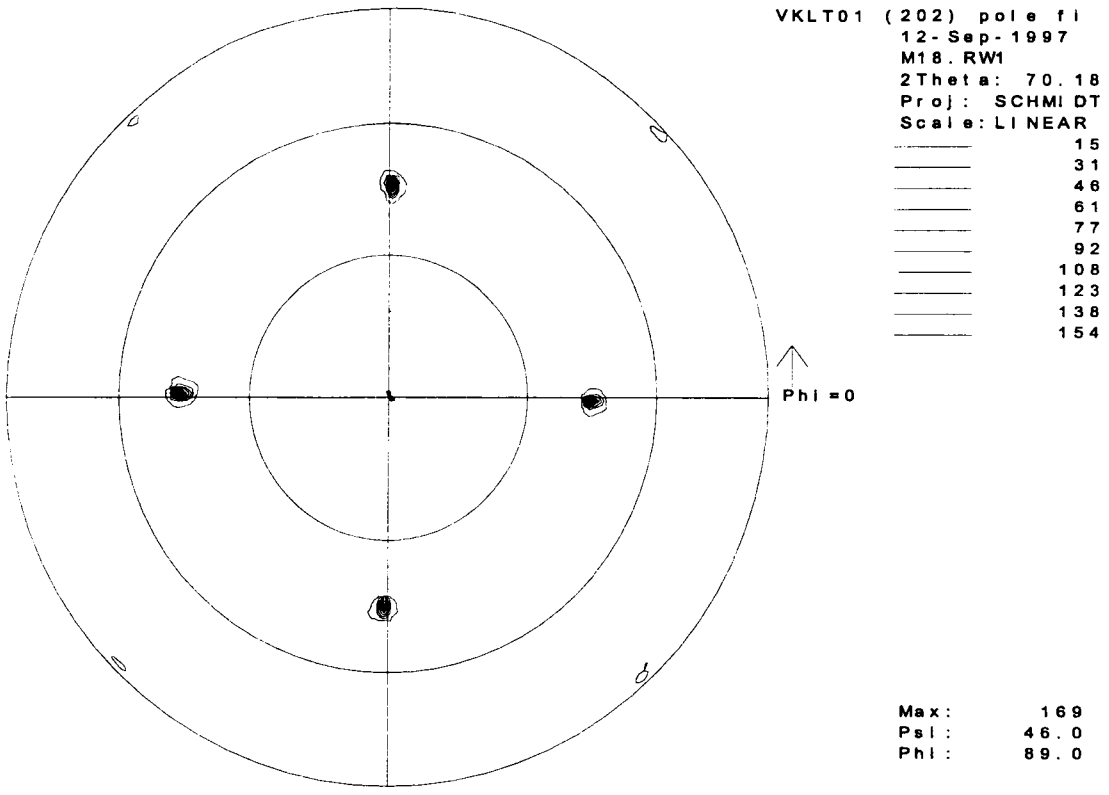


Figure 4.5: Typical Pole Figure for Epitaxial LAO/STO Film (VKLT 01)

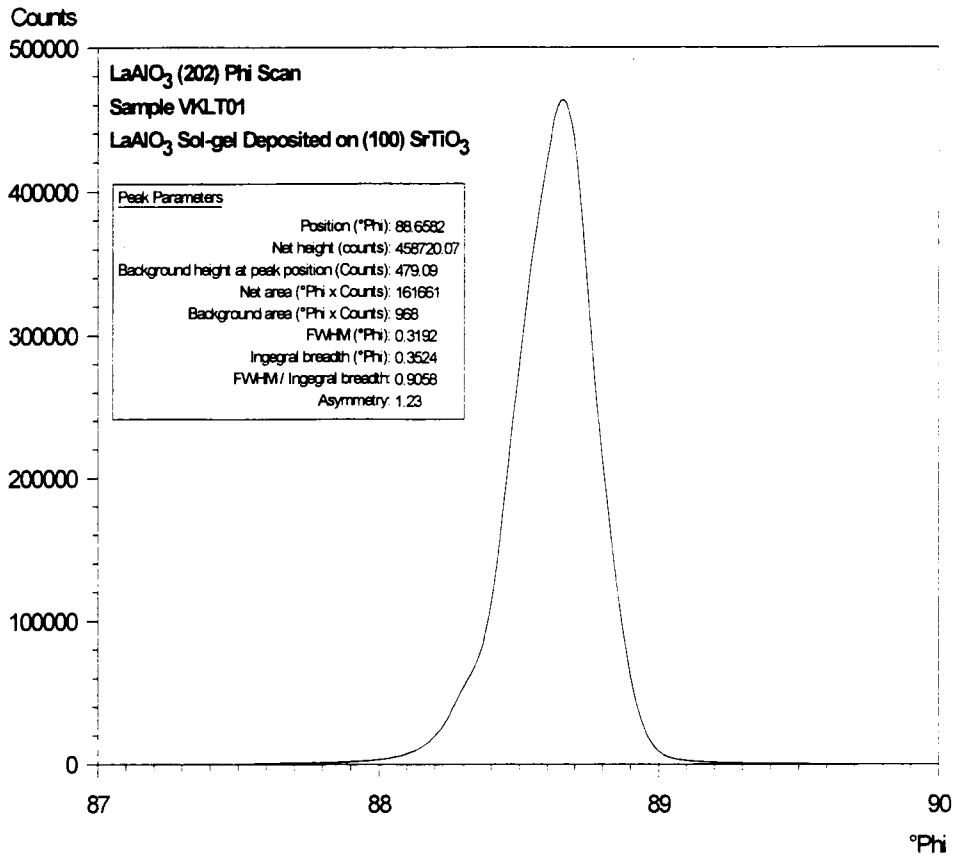


Figure 4.6: Typical ϕ Scan for Epitaxial LAO/STO Film (VKLT 01)

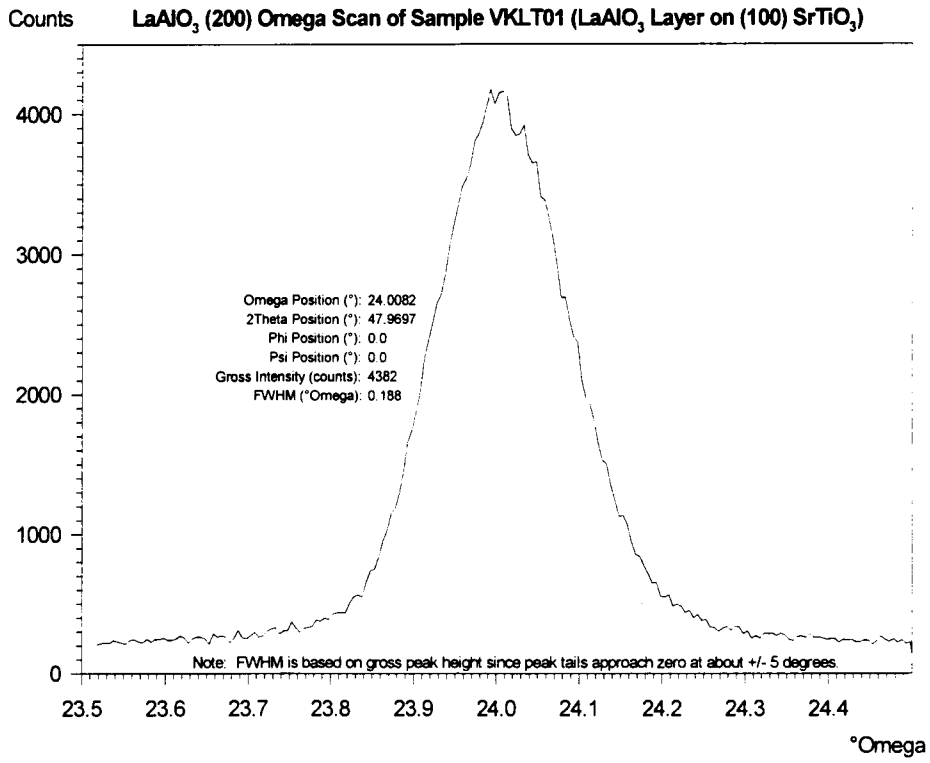


Figure 4.7: Typical ω Scan for Epitaxial LAO/STO Film (VKLT 01)

The FWHM value of 0.19 for ω scan verified the good c-axis alignment and the ϕ scan FWHM of 0.32 indicated that the film had a good in-plane texture.

4.3 Influence of Process Parameters on Film Texture for LAO/STO System

The samples were coated systematically by keeping a set of conditions the same (base conditions) for a particular set and varying only one of the parameters. The parameters under study included the solution, dipping and thermal processing variables. The base conditions were selected from prior knowledge of some of the most frequently used processing conditions. In particular, the effects of degree of hydrolysis - Dh (ratio of total molar cation concentration-to-moles of water), substrate withdrawal velocity - Vw (speed at which the substrate is withdrawn from the solution), thermal processing atmosphere - O_2 concentration, temperature - Ta , and processing time were studied. The coating was carried out as described in Chapter 3 and each sample was given an identification number. The results of the experiments on the LAO/STO system are shown in the Table 4-1. The effect of various parameters are then studied by gathering in the separate sets of samples with common base conditions.

Table 4-1: Experimental Data for LAO/STO System

Sample I.D	Dh	Vw (cm/min)	Ta (°C)	Time (min)	O_2 conc (vol. %)	FWHM Φ (deg)	FWHM ω (deg)
VKLT 01	1:1	3	800	5	21	0.34	0.19
VKLT 02	1:1	3	800	5	21	0.54	0.27
VKLT 03	1:1	33	800	5	21	0.46	0.28
VKLT 04	1:1	3	800	5	21	0.49	0.24
VKLT 05	1:1.2	33	800	5	21	0.35	0.19
VKLT 06	1:1.4	90	800	5	21	0.36	0.22
VKLT 07	1:1	3	700	5	21	0.36	0.24
VKLT 08	1:1	3	900	5	21	0.64	0.34
VKLT 09	1:1	3	800	1	21	0.44	0.20
VKLT 10	1:1	3	800	10	21	0.26	0.15
VKLT 11	NO DATA						
VKLT 12	1:1	3	800	5	100	0.28	0.16
VKLT 13	1:1	3	800	5	2	0.35	0.29
VKLT 14	1:1.2	3	800	5	21	0.34.	0.19
VKLT 15	1:1.4	3	800	5	21	0.33	0.18
VKLT 16	NO DATA						
VKLT 17	1:1	3	800	5	21	0.49	0.23

Table 4-1 Continued

Sample I.D	Dh	Vw (cm/min)	Ta (°C)	Time (min)	O_2 conc (vol %)	FWHM Φ (deg)	FWHM ω (deg)
VKLT 18	1:1.4	3	800	5	21	0.68	0.27
VKLT 19	1:1.4	33	800	5	21	0.86	0.41
VKLT 20	1:1.4	90	800	5	21	0.53	0.26
VKL62	1:1.4	3	900	10	< 50ppm* humidified	0.57	0.38
VKL64	1:1.4	3	800	10	<50ppm* humidified	0.61	0.38
VKL66	1:1.4	3	800	10	<50ppm*	0.69	0.31
VKL68	1:1.4	3	1100	10	<50ppm* humidified	0.75	0.30
VKL 115	1:1.2	3	800	20	21	0.40	0.34
VKL 116	1:1.2	15	800	10	21	0.88	0.23
VKL 117	1:1.2	33	800	10	21	0.82	0.23
VKL 118	1:1.2	70	800	10	21	1.10	0.45
VKL 119	1:1.2	90	800	10	21	0.96	0.56

* - A mixture of 4% H_2 in argon was used since this gas was generally used for thermally processing samples of LAO/Ni.

4.3.1 Effect of Degree of Hydrolysis (Dh)

The degree of hydrolysis is an indication of the moles of water available for the total La^{3+} and Al^{3+} cation concentration. An increase in the amount of water causes cross linking of the polymers in the sol-gel precursor solution. The base conditions are listed below and the influence of Dh on FWHM values is shown in Table 4-2. As can be seen in Figure 4.8 as the amount of water (i.e. Degree of hydrolysis, Dh) is increased the FWHM has a downward trend. This suggests that as expected an increase in Dh results in a better texture. The improved cross linking between La, Al and O atoms (increase in the size of the polymer) in the solution precursor results in a better texture during crystallization. Hence an increase in the degree of hydrolysis causes improved texture. However we cannot increase the degree of hydrolysis beyond 1:1.4 since that would generally cause instantaneous gelation of the precursor solution.

Base conditions

Solution parameters

Solution temperature = 20 °C

Viscosity = 2.5 cps

Dipping parameter

Withdrawal velocity = 3 cm/min

Thermal processing parameters

Temperature = 800 °C

Atmosphere = 21% O_2(Air)

Time = 5 min

Table 4-2: Effect of Degree of Hydrolysis on Film Texture of LAO/STO System

Dh	FWHM ω	FWHM ϕ
1:1	0.27	0.54
1:1.2	0.19	0.34
1:1.4	0.18	0.33

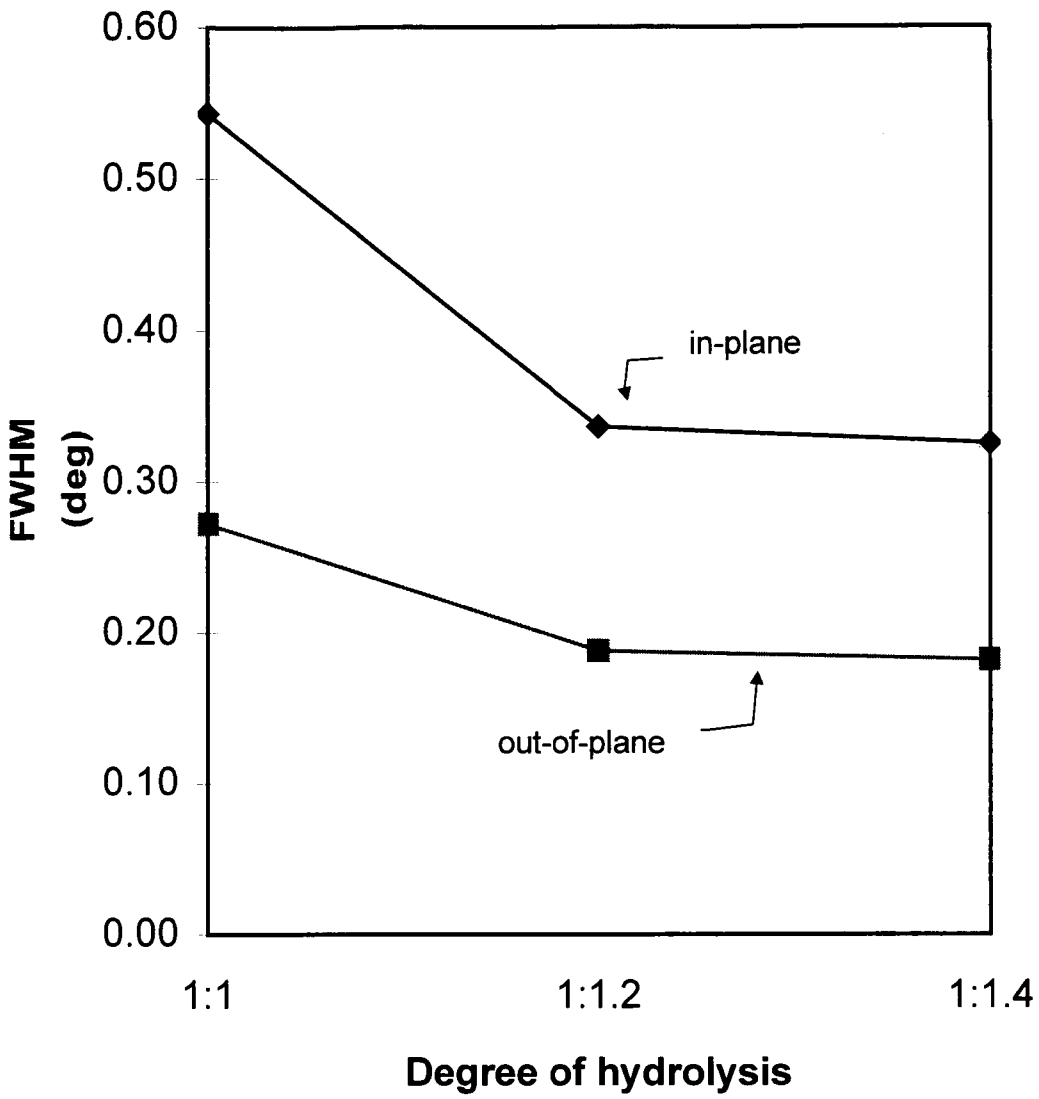


Figure 4.8: Effect of Degree of Hydrolysis on In-Plane and Out-of-Plane Texture for LAO/STO System

4.3.2 Effect of Withdrawal Velocity (Vw)

An increase in the withdrawal velocity results in a higher film thickness. As the thickness of the film increases the tendency to crack also increases. Also since one of the driving forces for epitaxial growth is controlled by the interface, as we go away from the interface there is a decline in the texture (and hence affects epitaxy). If one visualizes epitaxial growth as a layer by layer mimicking by the coating, the layer immediately in contact with the substrate will have the most superior texture compared to the surface of the coating. A study on the surface stress effects on thin film growth (Cammarata R.C. 1994) provides a relationship for the critical thickness for epitaxy for a layer-by-layer growth process. The basis of this derivation is that there is a critical thickness below which the equilibrium film-substrate interface is coherent, and above which it is thermodynamically favorable for misfit. The base conditions are listed below and the effect of Vw on film texture is shown in Table 4-3. As can be seen in Figure 4.9 as Vw is increased the FWHM has an upward trend. In other words as the film thickness increases, the texture of the coating deteriorates.

Base conditions

Solution parameters	**Thermal processing parameters**
Solution temperature = 20 °C	Temperature = 800 °C
Viscosity = 2.5 cps	Atmosphere = 21% O_2(Air)
Degree of hydrolysis = 1:1.2	Time = 5 min

Table 4-3: Effect of Withdrawal Velocity on Film Texture for LAO/STO System

Vw (cm/min)	FWHM ω (deg)	FWHM ϕ (deg)
3	0.34	0.40
15	0.23	0.88
33	0.23	0.82
70	0.45	1.10
90	0.56	0.96

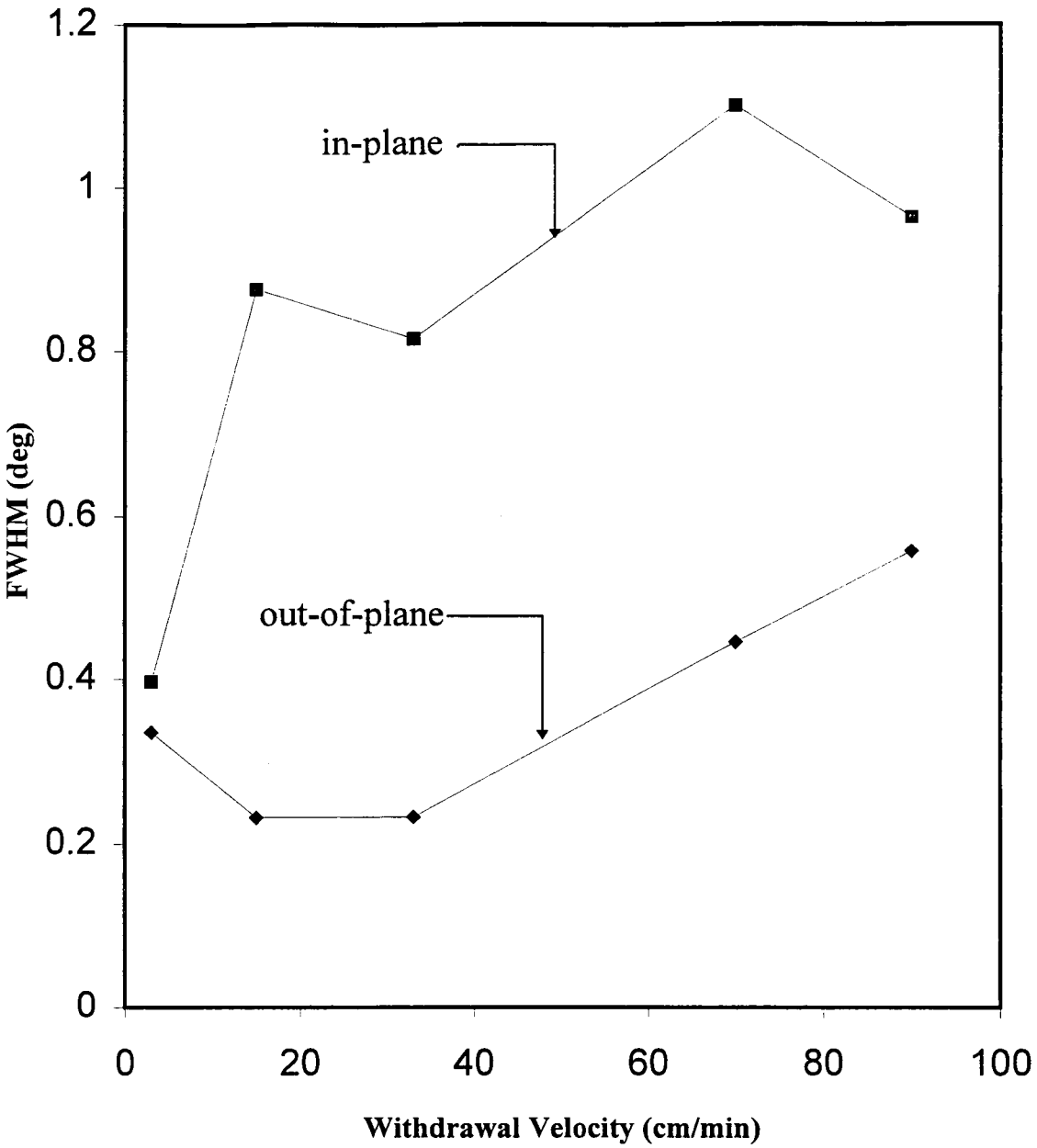


Figure 4.9: Effect of Withdrawal Velocity on In-Plane and Out-of-Plane Texture for LAO/STO System

4.3.3 Effect of Thermal Processing Atmosphere

The atmosphere most frequently used for processing the coated samples is air. The oxygen present in the air is responsible for the combustion of the carbon in the precursor and is also a source for the oxygen required for the thermal processing to achieve crystalline LAO. The base conditions are listed below and the effect of oxygen concentration on film texture is shown in Table 4-4 and Figure 4.10. As can be seen in the figure, as the atmosphere is changed from 100% O_2 to a mixture of 4%H_2 in Argon (thereby reducing the O_2 concentration to below 50 ppm) the FWHM values show an increasing trend which is indicative of texture deterioration due to lack of oxygen.

Base Conditions

Solution parameters

Solution temperature = 20 °C

Viscosity = 2.5 cps

Dipping parameter

Withdrawal velocity = 3 cm/min

Thermal processing parameters

Temperature = 800 °C

Time = 5 min

Table 4-4: Effect of Thermal Processing Atmosphere on Film Texture for LAO/STO System

O_2 (vol %)	FWHM ω (deg)	FWHM ϕ (deg)
100	0.16	0.28
21	0.27	0.54
2 *	0.29	0.35
<50ppm**	0.31	0.69

* - in argon
** - 4%H_2 in argon

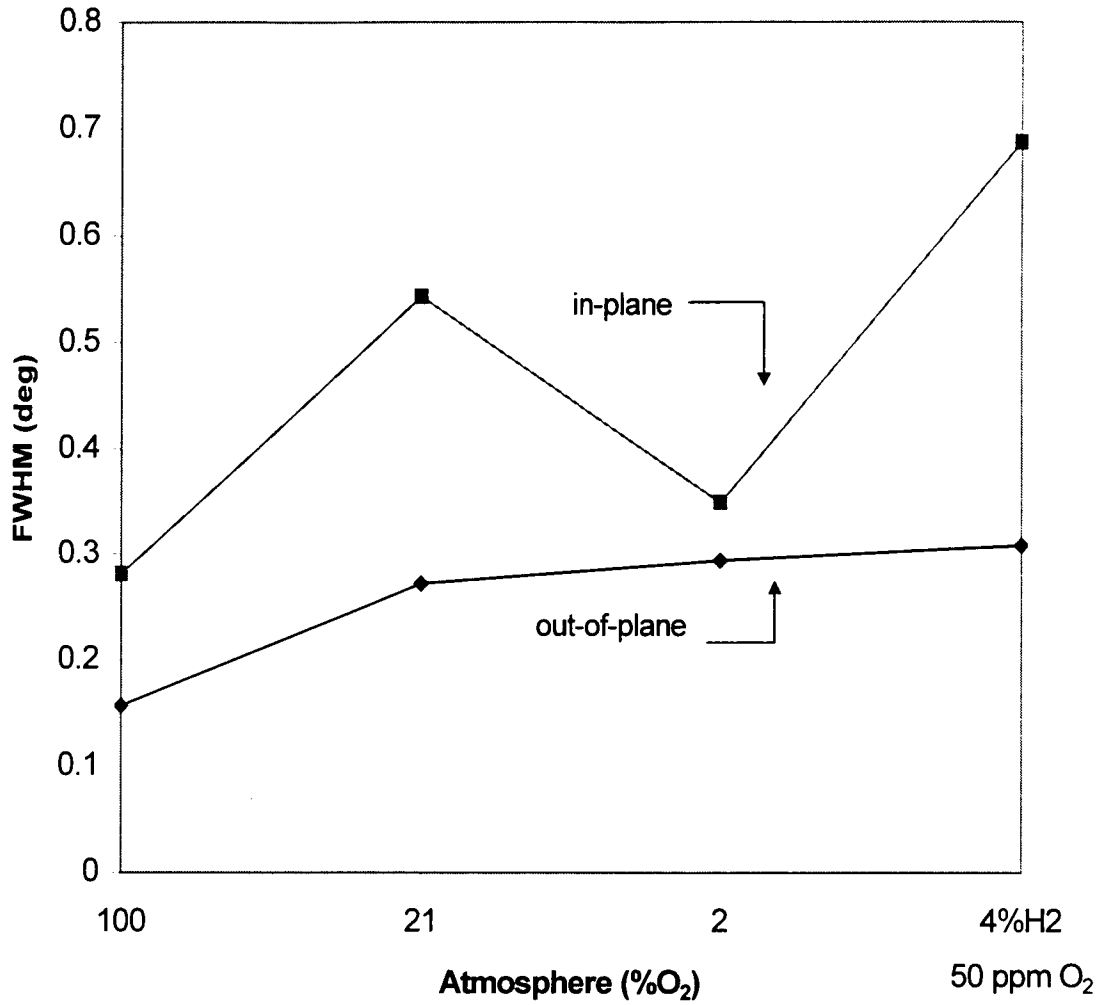


Figure 4.10: Effect of Thermal Processing Atmosphere on In-Plane and Out-of-Plane Texture for LAO/STO System

4.3.4 Effect of Thermal Processing Temperature

The crystallization temperature of ceramic oxides is generally higher than a few hundred degrees. The complete crystallization for LAO occurs at about 800°C. The experimental data is shown in Table 4-5 and the graphical representation of the same is in Figure 4.11. Although at 700 °C a low FWHM indicating a good texture was observed, it is most likely that complete crystallization may not have occurred yet and that there may be some amorphous phase left. Similarly, in this case it is possible that above 800°C a reaction may be taking place between the substrate and coating causing a deterioration in the texture. The experimental conditions are listed below.

Base conditions

Solution parameters

Solution temperature = 20 °C

Viscosity = 2.5 cps

Dipping parameter

Withdrawal velocity = 3 cm/min

Thermal processing parameters

Atmosphere (%O_2) = 21 (Air)

Time = 5 min

Table 4-5: Effect of Thermal Processing Temperature on Film Texture for LAO/STO System

Ta (°C)	FWHM ω (deg)	FWHM ϕ (deg)
700	0.24	0.36
800	0.27	0.54
900	0.34	0.64

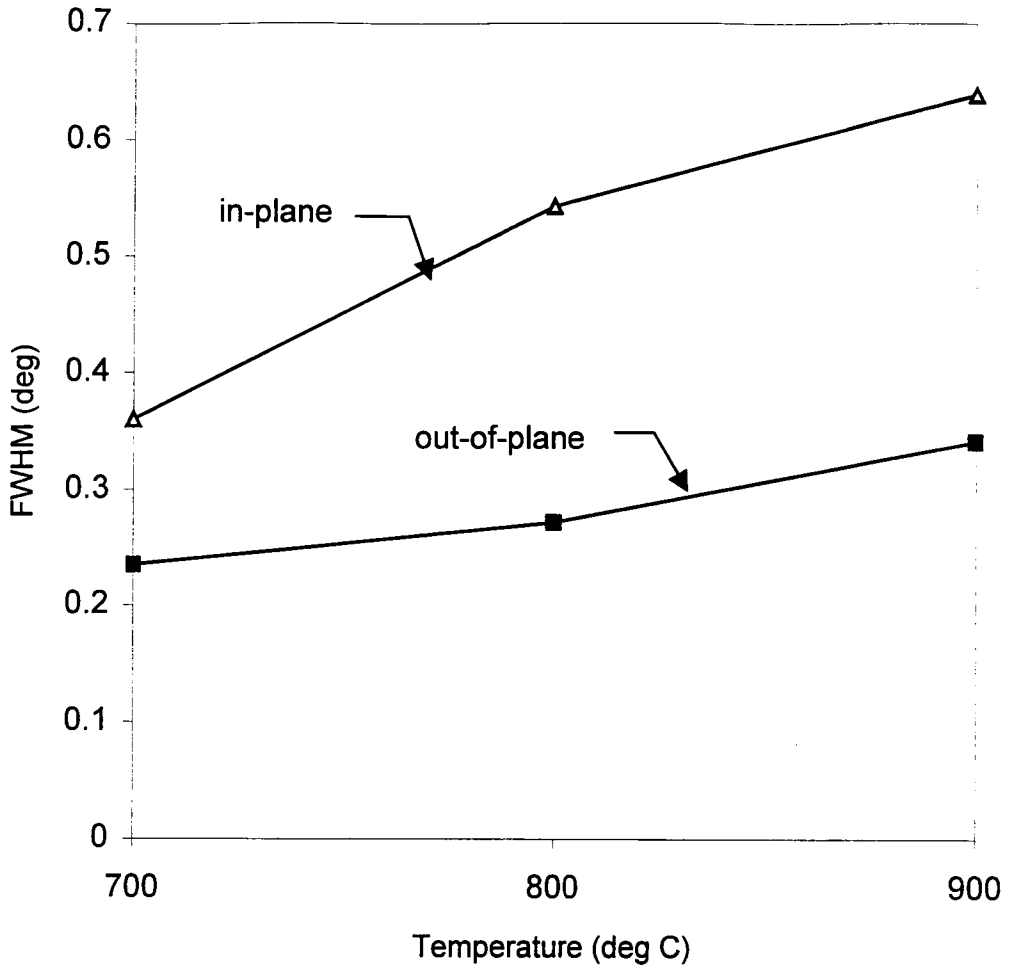


Figure 4.11: Effect of Thermal Processing Temperature on In-Plane and Out-of-Plane Texture for LAO/STO System

4.3.5 Effect of Thermal Processing Time

The experimental data for variation in FWHM values as a function of thermal processing time is given in Table 4-6. It can be seen in the graphical representation of this data in Figure 4.12 that as the processing time is increased the FWHM values reduced which means that a better texture is achieved with an increase in processing time. The crystallization process is basically an interphase mass transfer operation/reaction and hence should follow a general rate equation. As the processing time is increased the crystallization process tends to go to completion. However, this conclusion does not imply a monotonically improving texture with time. There is likely to be a deterioration of the texture after a certain time due to extended exposure at high temperature. The conditions used for the study are given below:

Base conditions

Solution parameters

Solution temperature = 20 °C

Viscosity = 2.5 cps

Dipping parameter

Withdrawal velocity = 3 cm/min

Thermal processing parameters

Atmosphere = 21 $\%O_2$

Temperature = 800 °C

Table 4-6: Effect of Thermal Processing Time on Film Texture for LAO/STO System

Time (min)	FWHM ω (deg)	FWHM ϕ (deg)
1	0.20	0.44
5	0.27	0.54
10	0.15	0.26

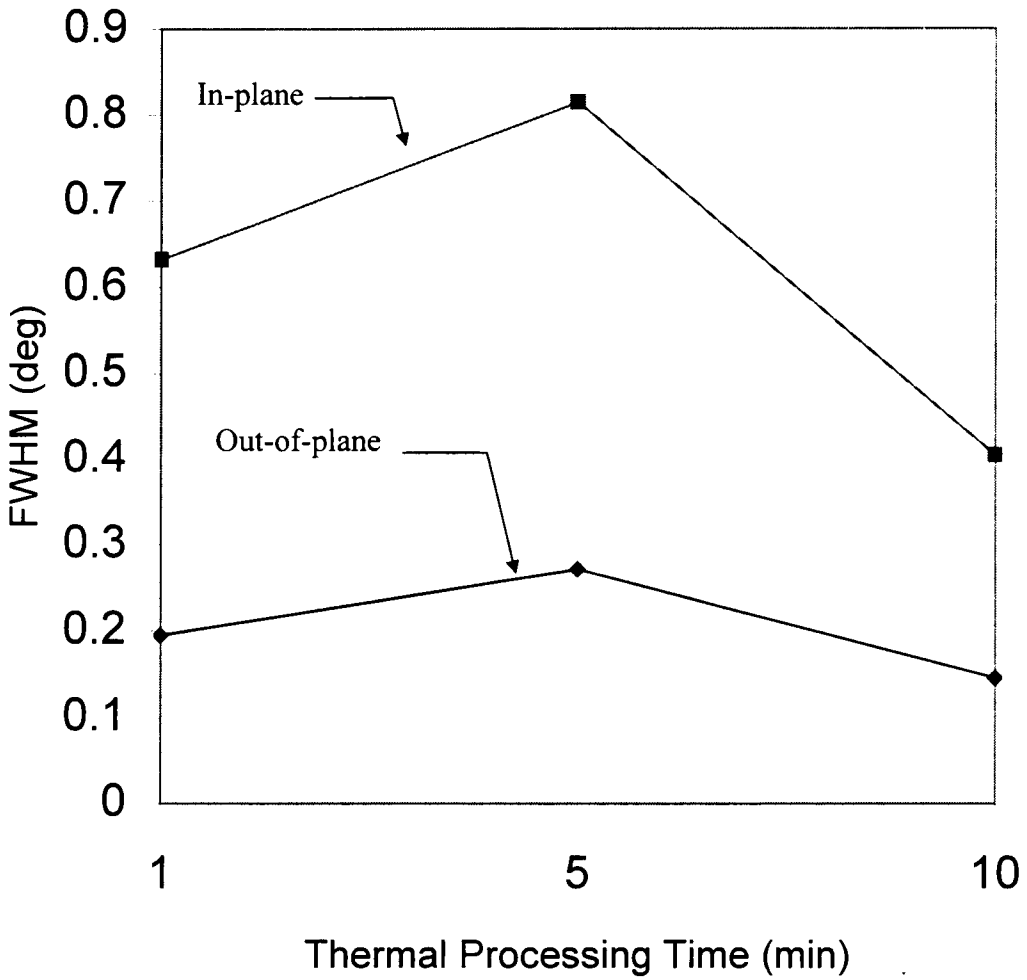


Figure 4.12: Effect of Thermal Processing Time on In-plane and Out-of-Plane Texture of LAO/STO System

4.4 Epitaxial growth of LAO on Ni(200)

Films on roll textured Ni were annealed at 1150 °C for 1 hour in flowing 4%hydrogen in argon (this atmosphere was used to prevent nickel oxide formation). A typical 2-theta XRD scan is shown in Figure 4.13. Only the (h00)- (where h is an integer which represents a crystal plane) peaks are prominent, although a small (110) peak can also be seen. The rocking curves for these films were also generated. Rocking curves (ω scan) about the (200) reflection had FWHM values of around 9-10°. Although this is significantly greater than the film deposited on single crystal STO, the values are similar to the FWHM values of the rocking curve for the nickel substrate itself about the (200) reflection (about 10°). To determine the degree of in-plane alignment, a pole figure about the (110) plane was obtained (see Figure 4.10). The eight-fold symmetry of the pattern indicates that there are two in-plane epitaxies-(LAO(100) || Ni(100) and LAO(110) || Ni(100)). The (110) epitaxy is rotated 45° from the cube-on-cube epitaxy. This pole figure analysis indicates that there are equal parts of both the epitaxies. Several process variations (which cannot be disclosed due to the proprietary nature of some work) were tried out with the aim of obtaining a single in-plane epitaxy. Due to the complex nature of the process, lack of subject matter in the field, inevitable process variations like nickel, humidity, and human error; the repetition of a favorable result was unpredictable. However, by closely controlling the process changes such as different batches of textured nickel supply, precursor solution, and processing conditions the effect of withdrawal velocity on the LAO/Ni system was studied.

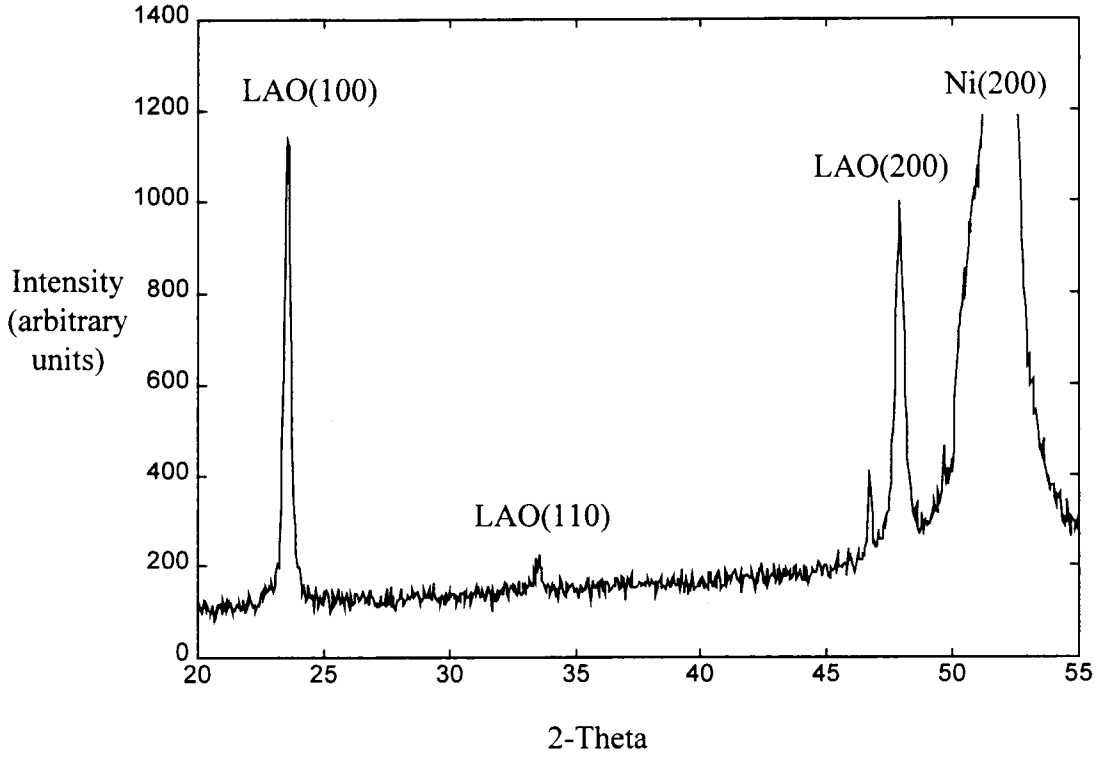


Figure 4.13: XRD Theta-2-Theta Scan for LAO/Ni Film

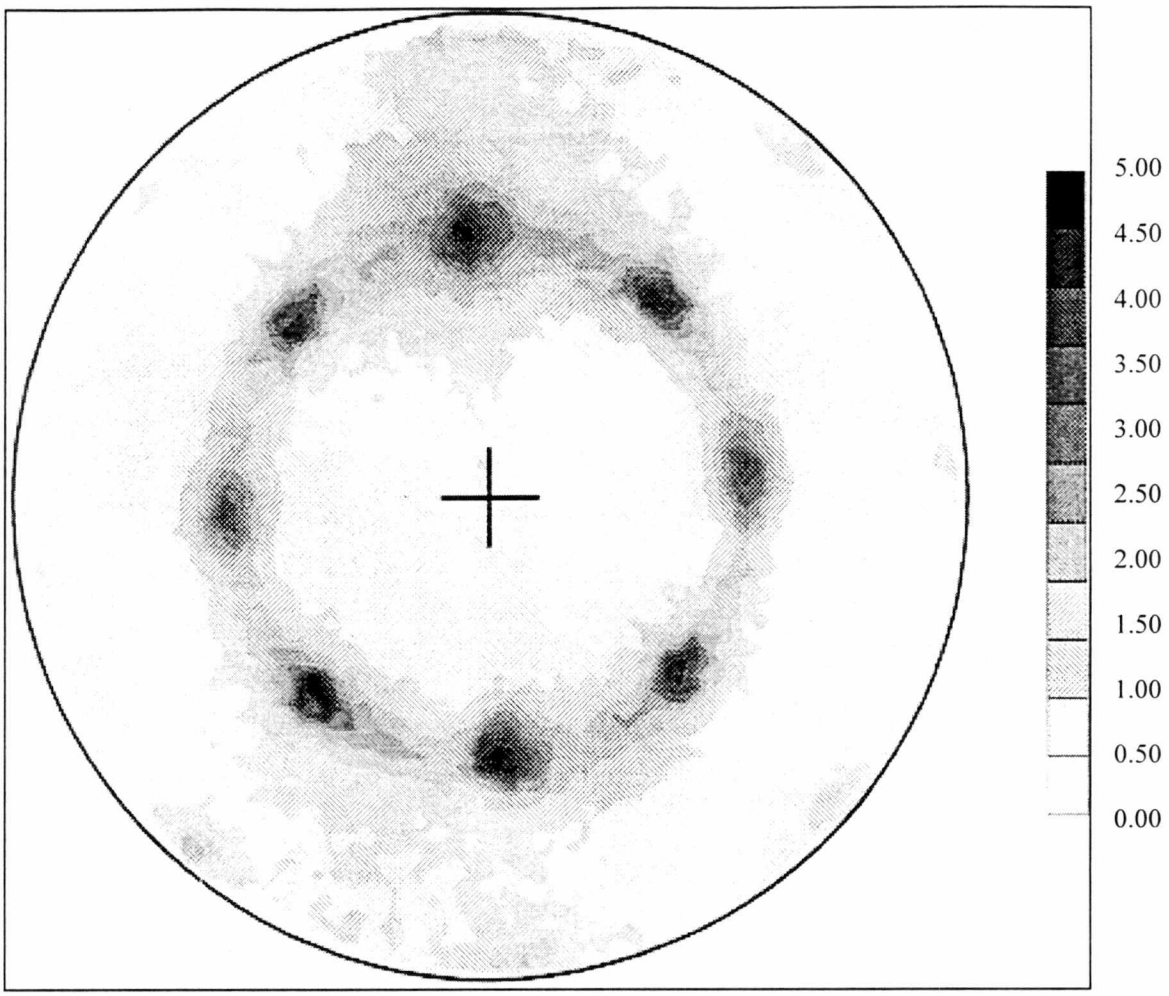


Figure 4.14: Pole Figure for LAO/Ni(200) Film

4.4.1 Effect of Withdrawal Velocity

Experiments were conducted on the epitaxial growth of LAO on textured nickel in a way similar to the LAO/STO system described earlier. However, only the effect of withdrawal velocity on the texture of LAO was studied. The conditions used for the study are shown below:

Base conditions

Solution parameters	**Thermal processing parameters**
Solution temperature = 20 °C	Temperature = 1160 °C
Viscosity = 2.5 cps	Atmosphere = 4% H_2 (in Argon)
	Time = 60 min

The experimental data generated is shown in Table 4-7 and Figure 4.15, there seems to be no significant change in texture with the change in the withdrawal velocity. This is unlike the behavior of the LAO/STO system described earlier. The growth of LAO on STO was 100 percent cube-on-cube texture, whereas that on textured nickel is only about 50 percent. A possible explanation for not observing a similar effect of withdrawal velocity as in the STO case may lie in the fact that the crystallization temperature required for epitaxial growth on Ni is 1150°C which is much higher than 800°C. Epitaxy is a thermodynamically governed phenomenon, and may be affected by this increase in temperature to an extent where the effects of increase of film thickness on texture are masked out by the possible thermodynamic temperature effect. In a study on the

Table 4-7: Effect of Withdrawal Velocity on Texture of LAO/Ni (200) System

Vw (cm/min)	FWHM ω (deg)	FWHM ϕ (deg)
1.5	9.46	14.6
3	10.46	17.60
3	8.67	12.1
6	9.72	13.32
9	11.24	16.67
12	9.24	11.99
15	9.77	16.69
30	14.2	18.68
45	9.77	15.6
45	11.72	20.82
60	11.84	15.22

Vw: Substrate withdrawal velocity (cm/min)

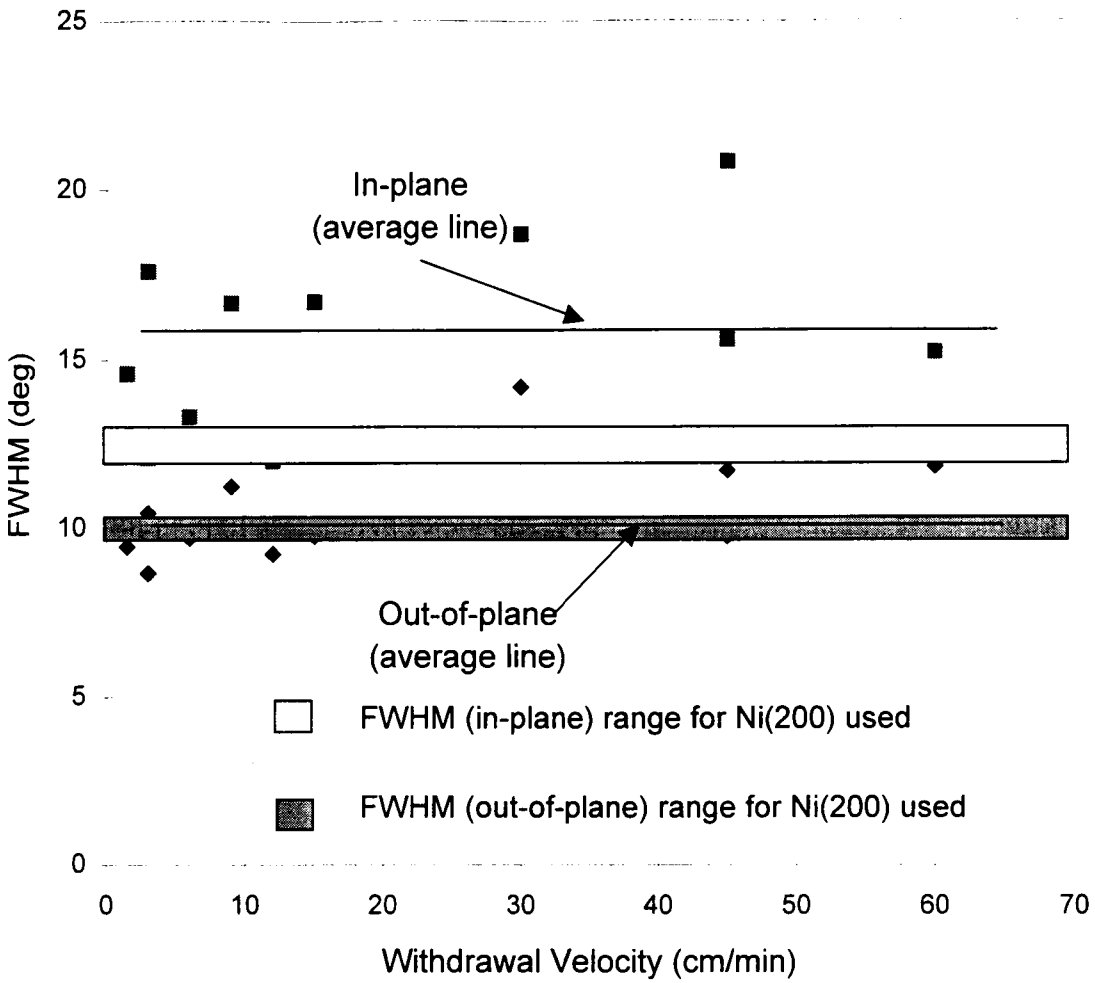


Figure 4.15: Effect of Withdrawal Velocity on In-plane and Out-of-plane Texture for LAO/Ni System

molecular dynamics of homoepitaxial growth on MgO(001) (Kubo M. *et al.* 1997), it was found that the substrate temperature is one of the important parameters to prepare well-defined MgO thin films. An increase in temperature resulted in a complete layer-by-layer homoepitaxial growth. However for the heteroepitaxial growth of Ag on MgO, a lower temperature was found to be favorable. Also surface defects in the MgO surface on the structure of the coating played an important role. Hence it is hypothesized that in the case of LAO/Ni system, factors such as temperature and surface of nickel may play a more important role than solution properties. Those parameters need to be optimized before any further optimization on the solution properties can be done.

4.5 Epitaxial Growth of YBCO Films on Single Crystal Substrates

Thin films of YBCO were grown epitaxially on single crystal substrates of LAO(100) and STO(100) by sol-gel and MOD methods. The thermal processing in this case is much more involved as compared to that in LAO/STO samples. The processed samples are first tested for room temperature resistance by a multimeter. As a rule of thumb, YBCO films are likely to have a critical temperature (T_c) around 90 K (which is close to the exact T_c of 91 K for YBCO) and exhibit a resistance in the 10-100 ohm range. The samples that showed a T_c in the superconducting region did indeed exhibit a room temperature resistance in the aforementioned range. The usefulness of this test was to decide whether to do T_c measurement on a sample because of the laborious and time consuming nature of such tests. The films were also tested by the XRD analysis to ascertain that the right phase (c-axis) orientation was achieved. Occasionally, some a-axis aligned material and

unwanted YBCO phases were also observed. But usually for the samples that exhibited T_c s in the right range this was not the case. A typical XRD theta-2-theta scan for a YBCO/STO sol-gel sample is shown in Figure 4.16. The peaks show strong c-axis orientation of YBCO. The YBCO(003) and YBCO(006) peaks overlap with the STO(001) and STO(002) respectively.

4.5.1 Critical Temperature Measurements on YBCO films

Critical temperature (T_c) measurements are necessary to ascertain the superconducting nature of the films and to decide if subsequent critical current density measurements are justified. T_c measurements were carried out on some of the best samples obtained. Figures 4.17-4.20, show the Resistance vs Temperature curves for four good samples. As a common practice instead of plotting the absolute resistance of the sample, the ratio of the resistance at temperature T-to-resistance at 300 K (room temperature) is plotted. The temperature at which the resistance drops to zero is the critical temperature. The current generally used for such measurements is 1 mA. However, once the test for T_c at 1 mA gives a good result the test is then redone at 200 mA. This is rule of thumb test to decide whether the sample is likely to exhibit a high critical current density. If the curves at the two different currents nearly superimpose it is possible that the sample may have a critical current density greater than 10^5 A/cm^2. One of the most important characteristics of the sample as far as achievable critical current density (J_c) is concrened is the atomic linkages of the YBCO. If there are very few weak linkages and less oxygen deficiency

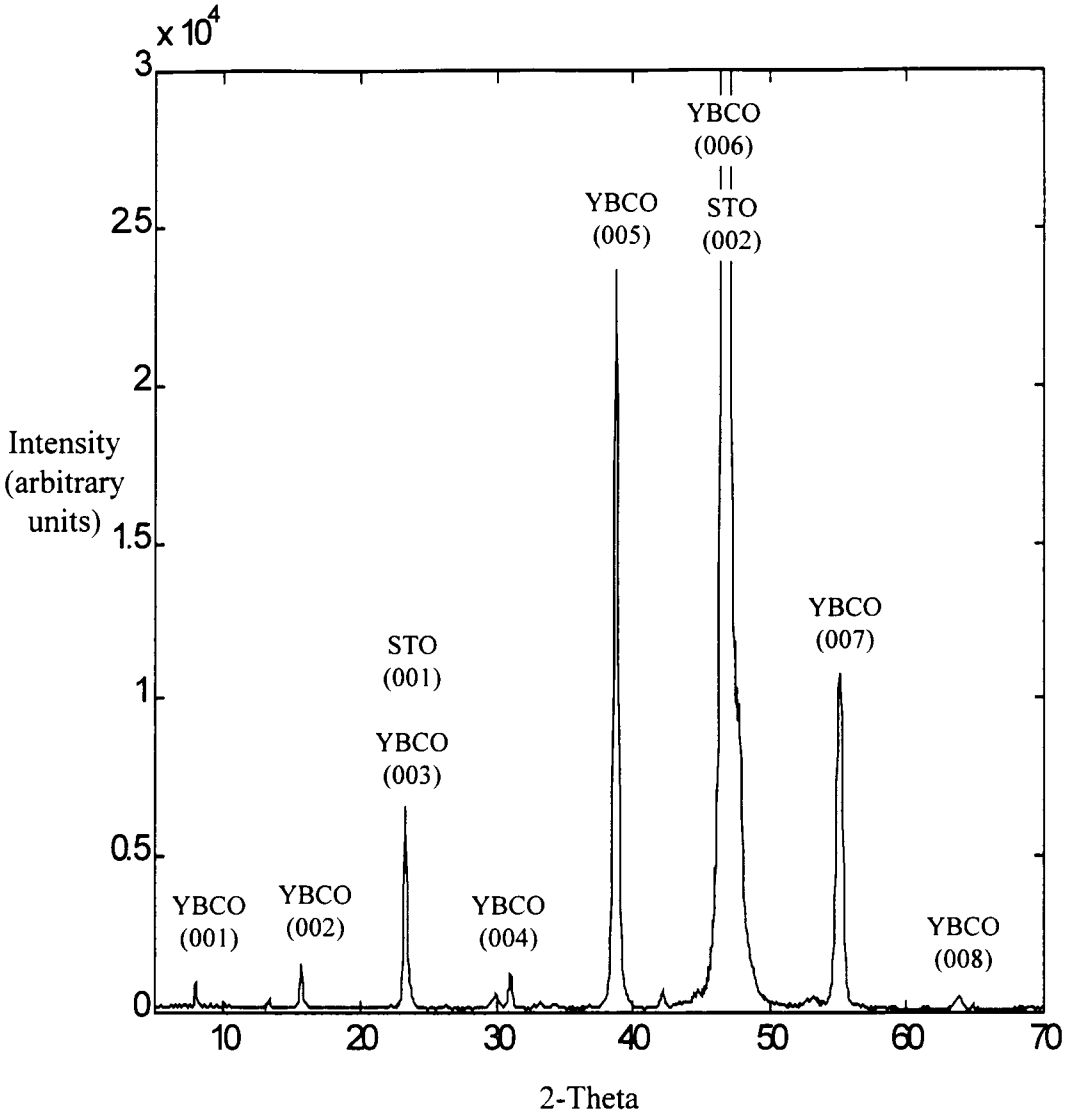


Figure 4.16 : XRD Theta-2-Theta Scan for YBCO/STO Sol-Gel Sample (VKL 87)

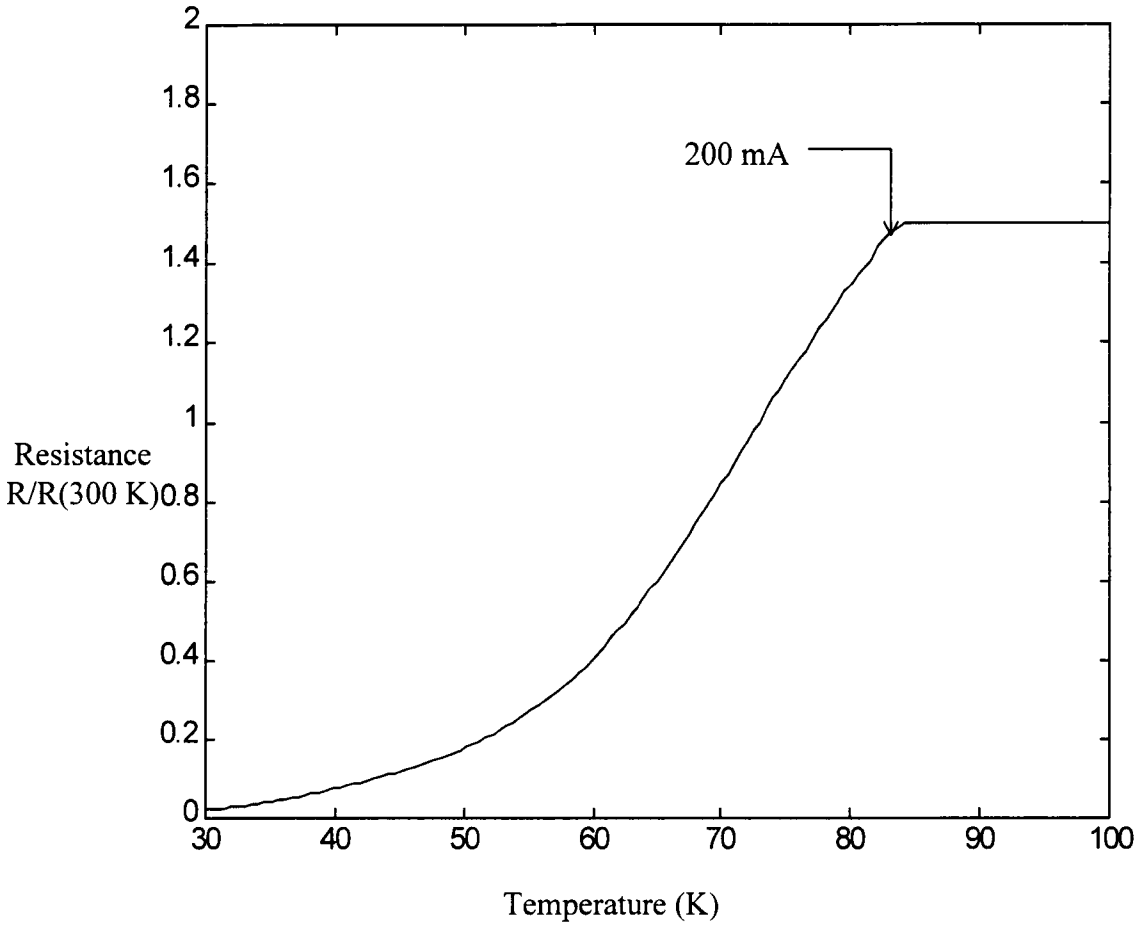


Figure 4.17: Resistance vs Temperature (K) for YBCO/STO Sample by Sol-Gel Route

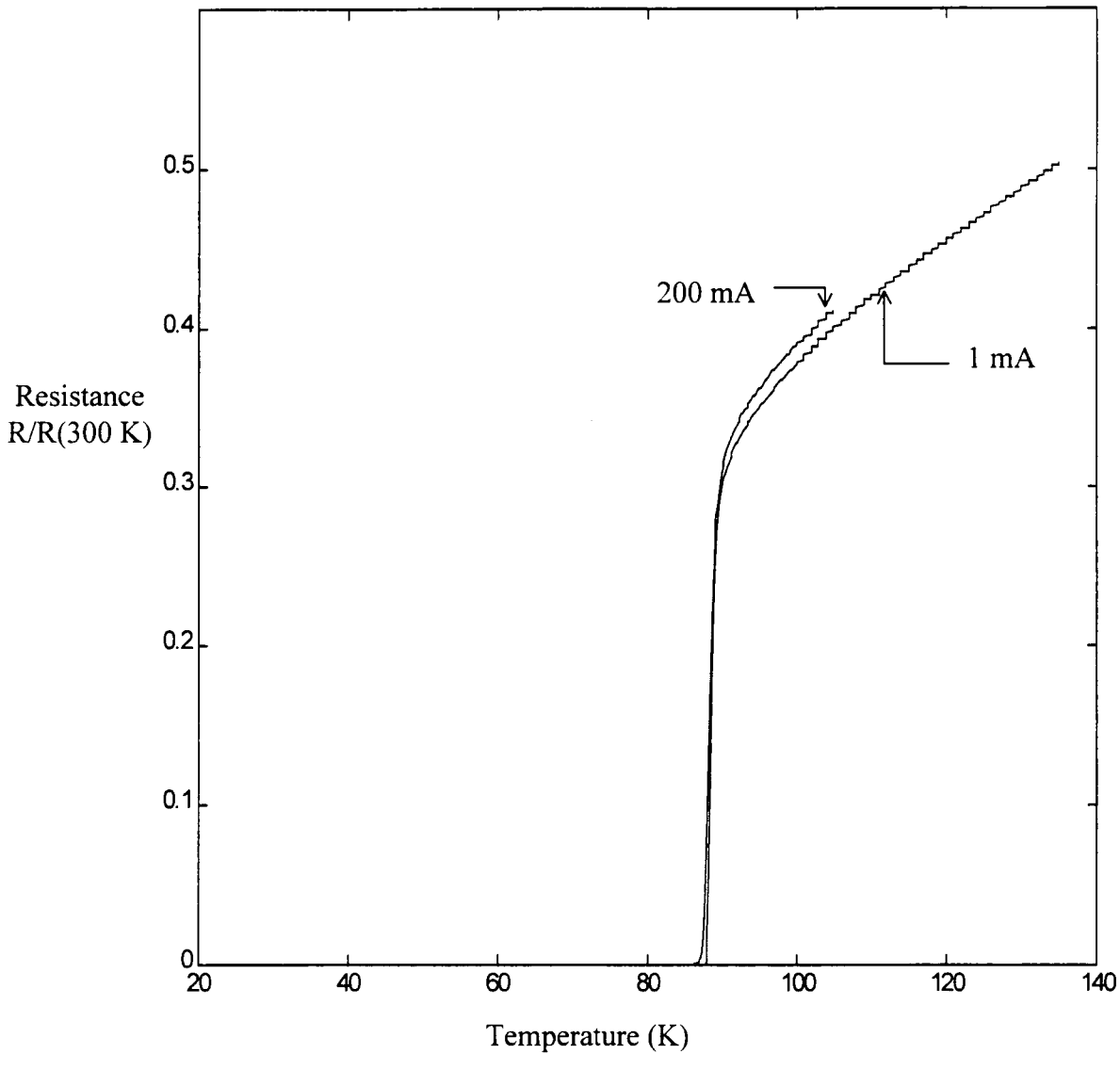


Figure 4.18: Resistance vs Temperature (K) for sample MOD 1 (YBCO/STO)

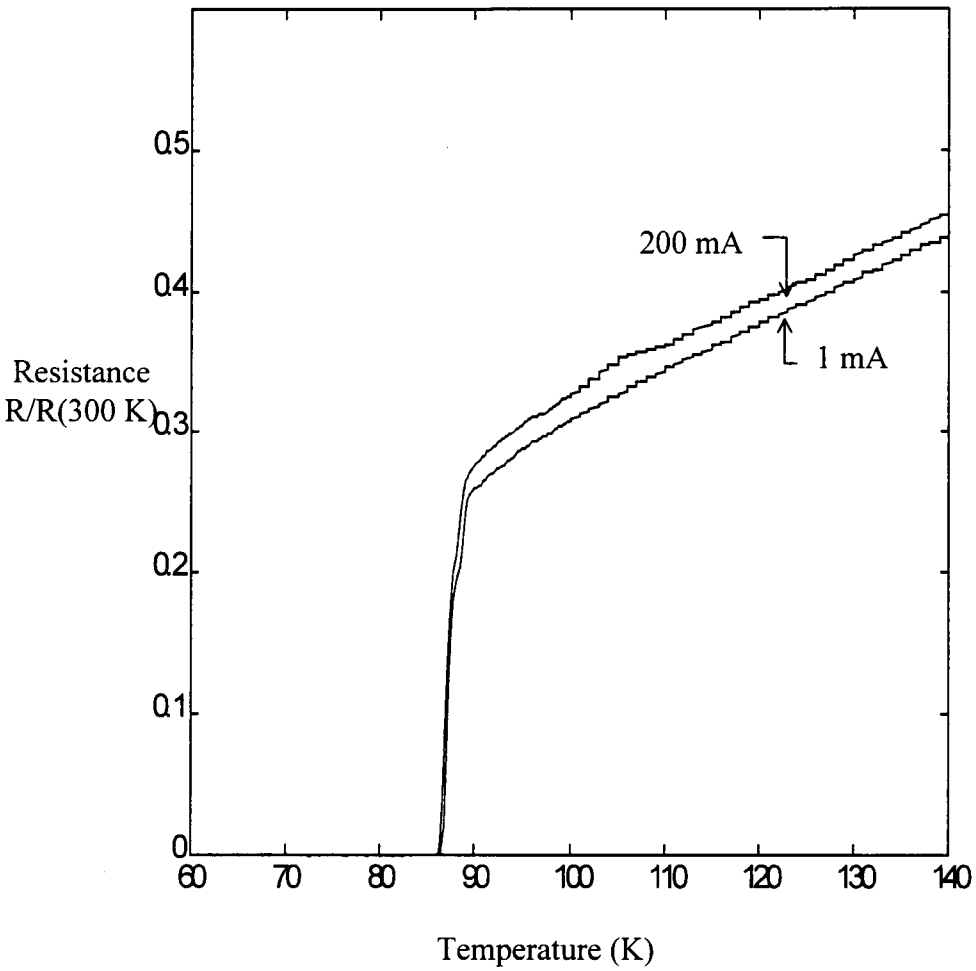


Figure 4.19: Resistance vs Temperature (K) for MOD 2 (YBCO/LAO)

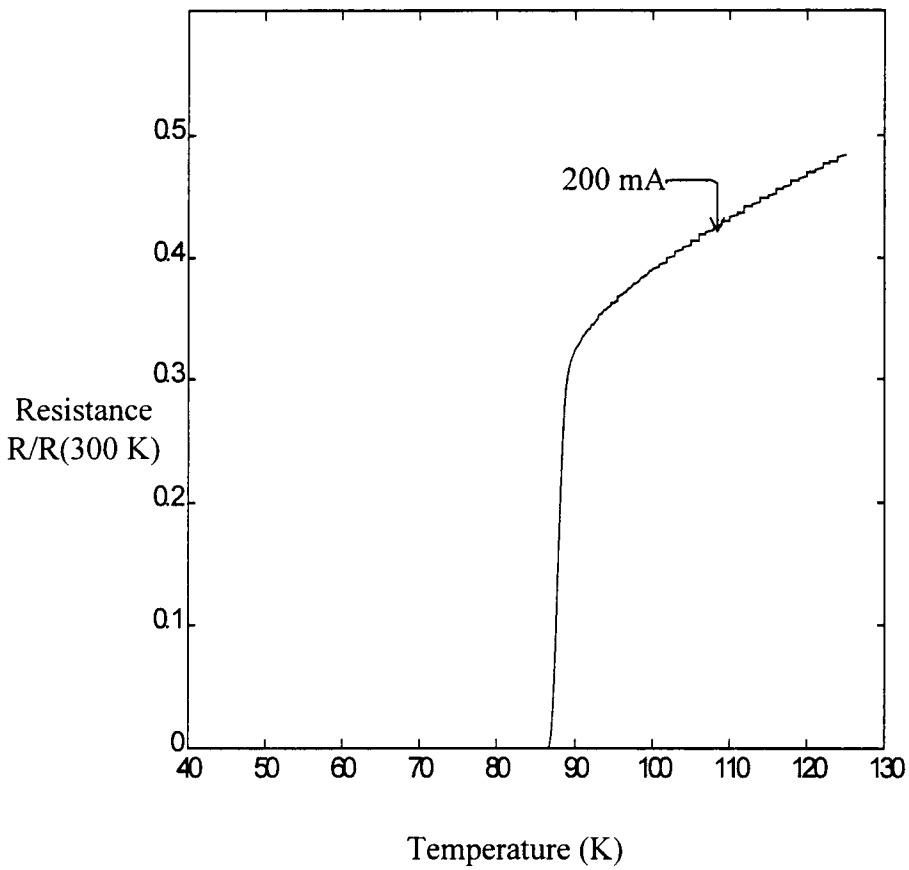


Figure 4.20: Resistance vs Temperature (K) for sample MOD 3 (YBCO/STO)

present then the samples would tend to sustain a higher current without significantly impeding the flow of electrons. This is the reason why the test at 200 mA is carried out.When there is no significant change in the T_c even with an increase in the magnitude of current it implies the linkages are strong and hence the sample will probably exhibit a J_c higher than 10^5 A/cm^2. The YBCO sample prepared by the sol-gel route did not show a good T_c probably because the stoichiometric ratio of Y:Ba:Cu was not exactly 1:2:3 which as a result may have caused the formation of unwanted phases. The flattening of the resistance curve after about 85 K was due to the resistance going out of range of measurement and hence does not represent the resistance of the sample. For samples MOD 1 and MOD 2 the measured T_c was in the 85-87 K range. A change in the current to 200 mA did not shift the T_c appreciable which indicated possibility of Jc around 10^5 A/cm^2 or more. To ensure proper reproducibility another sample was prepared using the same conditions and it also showed a T_c of about 87 K. The critical current density (Jc) was measured for the final sample (MOD 3).

4.5.2 Critical Current Density Measurement

The most important transport property of a superconductor is its ability to carry a super current without any heat dissipation. Hence once the T_c measurements indicate a prospect for a high J_c, measurement of J_c becomes imminent. The J_c also depends on various external parameters such as temperature and magnetic field. The temperature usually chosen is 77 K because it is the temperature of liquid Nitrogen. The dependence of J_c on

magnetic field is also determined because a lot of applications related to superconductivity require the superconductors to be under the influence of a magnetic field.. The dependency of J_c on magnetic field for this sample is shown in Figure 4.21. These measurements were conducted by the Solid State Division at ORNL. The highest J_c ($=1.81 \times 10^5$ A/cm^2) achieved in this work was that for the YBCO/LAO sample by MOD route (MOD 3). The rapid fall in J_c with an increase in magnetic field is a likely indication of weak linkages between the atoms of Y, Ba, Cu and O in the YBCO film. The solution properties of the MOD precursor solution should be adjusted to ensure better linkages in the film. An increase in the concentration of the solution is one of the most obvious parameters that can be changed. However, an increase in concentration may result in an unstable solution and possible precipitation of one or more of the salts out of the precursor solution which is not favorable. Hence the success of the solution techniques seems to lie in balancing the solution properties to optimize the desired properties of the superconducting film.

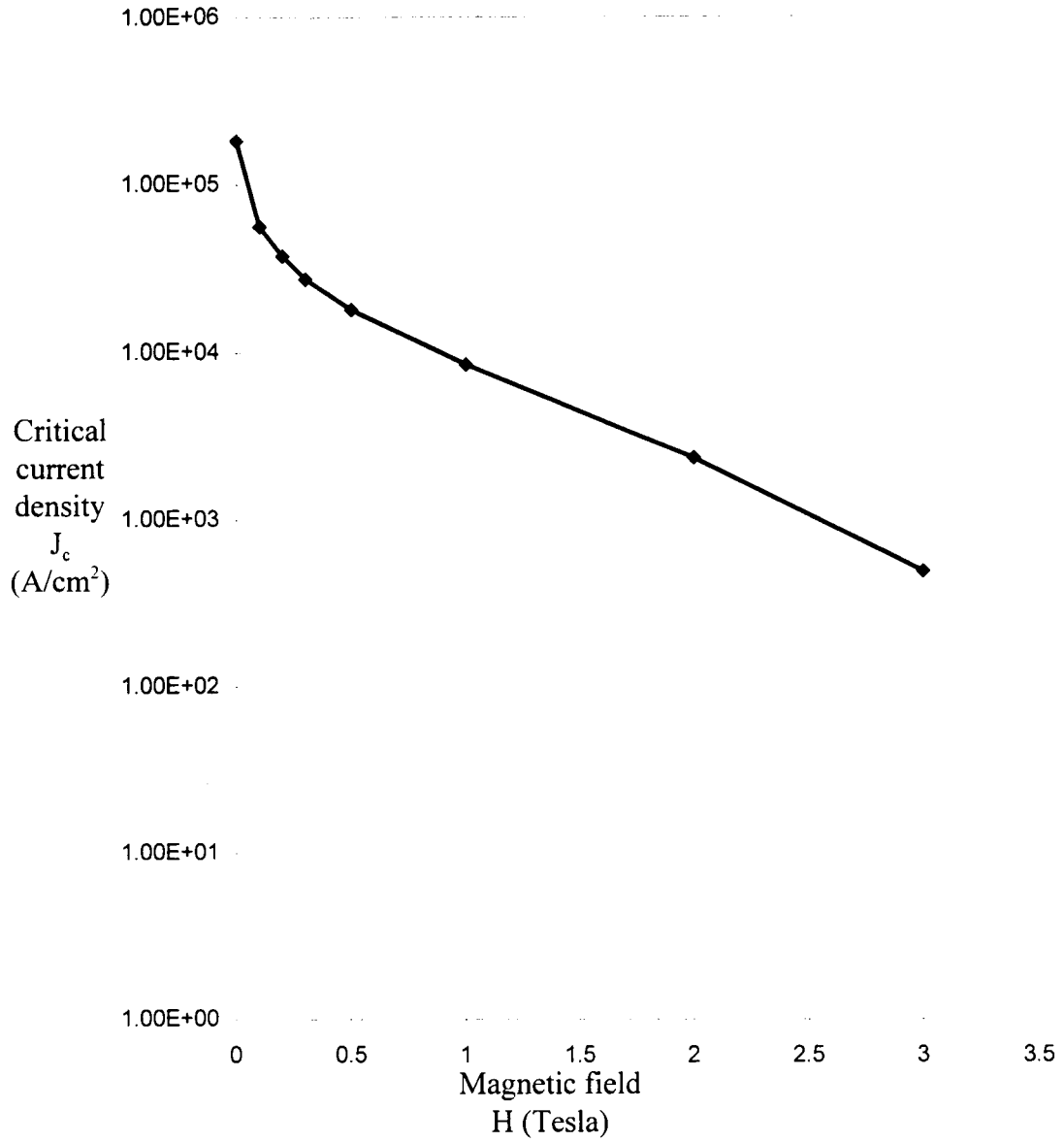


Figure 4.21: Effect of Magnetic Field on J_c (MOD 3)

Chapter 5

Summary and Conclusions

5.1 LAO/STO System

Single crystal substrates of STO (100) (5 x 10 mm) were coated with LAO sol-gel precursor solution by dip-coating. LAO grows epitaxially on STO (cube-on-cube texture). This was confirmed by the pole figure analysis. Rocking curves were used to study the texture of the coatings. The FWHM values for in-plane texture ranged from 0.26 (VKLT 10) to 1.10 (VKL 118) and out-of-plane from 0.15 (VKLT 10) to 0.56 (VKL 119). The influence of solution, dipping, and thermal processing parameters on the in-plane and out-of-plane texture of the coatings was studied. An increase in withdrawal velocity appears to deteriorate texture while an increase in degree of hydrolysis, thermal processing time and temperature and oxygen concentration seemed to improve texture. Based on the the limited work carried out, the optimum conditions recommended for the growth of epitaxial LAO on STO include:

Dh = 1:1.4

Vw = 3.1 cm/min

Ta = 800°C

Time = 10 min

O_2 = 100% (pure oxygen)

These parameters are not based on any rigorous mathematical optimization process but are based on the best combination of the conditions giving the most desirable results.

Bench scale dip-coating proved to be a useful technique for the sol-gel method. For lengths longer than 1 cm dip-coating should be a more effective way of producing films with uniform thickness. The thickness of most of the films grown seems to be in the vicinity of a 1000 $\mathring{A}$. Also to manufacture long-length samples the dip-coating system should be easy to scale up without much complication.

5.2 LAO/Ni System

Once the epitaxial growth of LAO on STO (100) was achieved, the next step was to study the epitaxial growth of LAO on textured Ni. A number of separate studies have been carried out by using different samples of RABiTS Ni obtained from the Metals and Ceramics Division of ORNL. The process for textured Ni is still under development and constantly changing and this complicates the systematic study on the LAO/Ni system. The studies involved varying the degree of hydrolysis of the precursor and processing conditions. Only the effect of withdrawal velocity on the in-plane and out-of-plane texture of the coatings was studied. In this case withdrawal velocity did not have much of an effect on the texture probably because the epitaxial growth mechanism is more dependant on the thermodynamics of the process. Epitaxy is a thermodynamically governed phenomenon because the driving force for epitaxy is the attainment of minimum energy. The free energy of epitaxial growth of the buffer layer, like any

chemical process is dependent on temperature. In this case other factors, such as texture of the substrate, lattice mismatch between the substrate and the buffer layer, thickness of the film would also play a role in the epitaxial growth. It is possible that for the LAO/Ni system, the temperature, substrate texture and lattice mismatch probably control the epitaxy more than the thickness of the film. Hence the effect of film thickness on texture of the coating may not very visible because the change of substrate from STO to textured Ni, makes the other factors like temperature, substrate texture and lattice mismatch take control of the epitaxial growth. The study of dip-coating on LAO/Ni system however achieved two main objectives:

1.The epitaxial growth of LAO on textured Ni had already been achieved at ORNL. The present study while giving further insights into this system also explored the dip-coating approach which is easily scalable. The two systems i.e. LAO/STO and LAO/Ni differed in that 100% epitaxial growth was achieved in the first case as against 50-70% for the latter.

2. A study of the dependency of the coating texture for the LAO/Ni system on withdrawal velocity did not show any significant change in texture with change in withdrawal velocity as the LAO/STO system showed.

Further studies to gain insight into the epitaxial growth are required. This may involve sophisticated instrumentation like a high temperature x-ray diffractometer that analyzes the growth of the coating as a function of parameters like time and temperature.

5.3 YBCO/STO and YBCO/LAO Systems

Superconducting films of YBCO were grown epitaxially on STO (100) and LAO (100) single crystal substrates following the MOD route. YBCO films were also grown by following the sol-gel route, however this particular film was not superconducting. The low solubility of the copper precursor is probably the main reason for poor results obtained by the sol-gel method. However, there lies potential in this method with meticulous experimental techniques in adjusting the ratios of Y:Ba:Cu to the required amount (1:2:3). The balance between trying to get the right stoichiometry while trying to make the solution stable is very critical for the success of most of the solution techniques for making YBCO. Differential Thermal Analysis (DTA) can prove to be a very useful tool in preparing the solutions and adjusting the stoichiometry.

Critical temperatures achieved for YBCO samples were around 90 K. J_c could not be measured for all the samples because the dimensions of the sample did not conform to the standards for measurement. However the J_c was measured for one sample (VKYB 15). The J_c for this sample was high and was equal to 1.81×10^5 A/cm^2 at 77 K and zero field. The effect of magnetic field on J_c reveals a drop in J_c with an increase in the magnetic field. The probable reason for this behavior is attributed to the weak linkages (bonds) in the crystal structure of the grown YBCO film. The MOD method proved to be a simpler method for growing YBCO films with high critical current densities. However further work is needed to reach the target J_c of 1 MA/cm^2 or greater on textured Ni. Also, the possibility of using dip-coating for this method needs to be further explored.

Chapter 6

Recommendations

6.1 YBCO on LAO/STO and LAO/Ni

Following the solution growth techniques the epitaxial growth of LAO was achieved for LAO on STO (100) single crystal substrates and also for YBCO on LAO(100) and STO(100) single crystal substrates. Hence the next step is to combine the two ideas and grow YBCO on LAO/STO films formed by the sol-gel method. A high critical current density (J_c) was achieved on one sample of superconducting YBCO film grown on single crystal substrate of LAO. If one is able to achieve a similar or higher value of J_c on YBCO films grown on the substrate with a buffer layer, it should show a good prospect for YBCO films grown on textured nickel substrates with a buffer layer. Once J_cs of the order of 1 MA/cm^2 are achieved on the LAO/STO films, the following step should be to achieve this target for similar films grown on the LAO/Ni films. A variety of options exist in optimizing the final properties of the superconducting tape. These include starting out with different precursors that have higher solubilities in the same solvent, and optimizing the time-temperature and atmosphere program for processing the samples.

6.2 Combination of Different Methods

Although it was planned to carry out some experiments based on the following approach, constraints of time and optimum results (i.e. best results on single crystal substrates) proved to be obstacles. Buffer layers and superconductor films are grown by several

methods as mentioned in Chapter 2. It is not necessary that if the buffer layer is grown by one technique, that the superconductor also needs to be grown by the same. A combination of different techniques may prove to be a viable option. Some of the combinations possible are:

1. YBCO grown by MOD method on a buffer layer which is grown on textured nickel by some of the state-of-the art technique. The techniques to grow buffer layers and superconductors are constantly evolving and hence the best suited option should be explored.

2. YBCO grown on LAO(grown by sol-gel)/Ni (RABiTS). The YBCO can be grown by any technique that has proven successful on single crystal or other substrates. The BaF_2 process which uses e-beam for making YBCO films at ORNL is one such technique.

6.3 Long Length Samples

The coated sample lengths generally were around 8 mm for the single crystal substrates and 8 - 15 mm for textured nickel. The advantages of making a sample of long length (> 2 mm) are two-fold:

1. The area with uniform coating would increase because of the reduction in the percentage of the unevenly coated ends and therefore the end effects.

2. Long length samples with high critical current density would enhance industrial interest in the solution based growth techniques.

Hence the dip-coating unit needs to be modified to enable coating long length samples.

LIST OF REFERENCES

LIST OF REFERENCES

1. Sheahen, T.P., "Introduction to High-Temperature Superconductivity," Plenum Press. New York, 1994.

2. Bednorz, J.G., and K. Mueller, *Z. Phyzik*, **B64**, 189(1986).

3. Goyal, A., D.P. Norton, D.M. Kroeger, D.K. Christen, M. Paranthaman, E.D. Specht, J.D. Budai, Q. He, B. Saffian, F.A. List, D.F. Lee, E. Hatfield, C.E. Klabunde, P.M. Martin, J. Mathis and C. Park, to be published in *J. Mater. Res.*, Special Issue, celebrating 10th anniversary of HTS, November 1997, 1-9(1997).

4. Krause, C., Oak Ridge National Laboaratory Review, **29**,3&4, 2(1996).

5. University of Tennessee Space Institute (UTSI), "Evaluation of Methods for Application of Epitaxial Buffer and Superconductor Layers," a report prepared by UTSI for DOE under Contract No. DE-AC22-95PC95231, 1998.

6. "Technology 1997 Analysis and Forecast," reprint from *IEEE Spectrum*, **34**, 1, 39(1997).

7. "HTS Wire Development Workshop," Conference Proceeding, January 31- February 1, 1996.

8. Paranthaman, M., *Personal Communication*, 1996.

9. Owens, F.J., and C.P. Poole Jr., "The New Superconductors," Plenum Press, New York, 1996.

10. Wu, X.D., S.R.Foltyn, P.N. Arendt, W.R. Blumenthal, I.H. Campbell, J.D. Cotton, J.Y. Coulter, W.L. Hults, M.P. Maley, H.F.Safar, and J.L. Smith, *Appl. Phys. Lett.* **67**(16), 2397(1995).

11. Shoup, S.S., M. Paranthaman, and D.B. Beach, *J. Mater. Res.*, **12**, 4, 1017(1997).

12. Peshev, P., and V. Slavova, *Mater. Res. Bull.*, **29**, 3, 255(1994).

13. Budd, K.D., S.K. Dey, and D.A. Payne, *Brit. Ceram. Proc.*, 36, 107(1985).

14. Paranthaman, M., and D.B. Beach, *J. Am. Ceram. Soc*, **78**, 9, 2551(1995).

15. Sun, Y., and I. Oh, *Ind. Eng. Chem. Res.*, **35**, 4296(1996).

16. Singhal, A., M. Paranthaman, E.D. Specht, R. D. Hunt, D.B. Beach, P.M. Martin, and D.F. Lee, " Solution Processing of $YBa_2Cu_3O_{7-x}$ Thin Films," to be submitted, 1(1998)

17. McIntyre, P.C., M.J. Cima, and M.F. Ng, *J. Appl. Phys.*, **68**, 8, 4183(1990).

18. McIntyre, P.C., M.J. Cima, J.A. Smith Jr., R.B. Hallock, M.P. Siegal, and J.M. Phillips, *J. Appl. Phys.*, **71**, 4, 1868(1992).

19. Francis, L.H., "Sol-Gel Processing, Perovskite Phase Development and Properties of Reloxor-Based Thin Layer Ferroelectrics," Ph.D Dissertation, University of llinois at Urbana-Champagne, 36(1991).

20. Brinker, C.J, C. Ashley. R.A. Cairncross, K.S. Chen, A.J Hurd, S.T. Reed, J. Samuel, P.R. Schunk, R. W. Schwartz, and C.S. Scotto, in "Metallurgical and Ceramic Protective Coatings,", edited by K.H. Stern, Chapman & Hall, London, pp. 114, 118, 125(1996).

21. Beach, D.B., M. Paranthaman, and C.E. Vallet, "Solution Routes to Multi-Cation Epitaxial Oxide Thin Films," to be submitted. 1997

22. Kister, S.F., and P.M. Schweizer, "Coating Science and Technology: An Overview," in "Liquid Film Coating," edited by S.F. Kister and P.M. Schweizer, Chapman & Hall, London, 1st edition, pp. 10, 1997.

23. Brinker C.J., and A.J. Hurd, "Fundamentals of Sol-Gel Dip-Coating," *J. Phys. III. France*, **4**,1231(1994).

24. Li, K.K., G.H. Haertling, W. Howng, *Integrated Ferroelectrics*, **3**, 81-87(1991).

25. Middleman, S., "Fundamentals of Polymer Processing," Mc-Graw Hill, Inc., pp. 212, 1977.

26. Brinker, C.J., and G.W. Scherer, "Sol-Gel Science," Academic Press, Inc., pp. 795., 1990.

27. Cullity, B.D., "Elements of X-Ray Diffraction," 2nd edition, Addison-Wesley Publ. Co., pp. 297,1978.

28. Feenstra, R. T.B. Lindemer, J.D. Budai, and M.D. Galloway, *J. Appl. Phys.*, **69**(9), 6569(1991).

29. Cammarata, R.C., *Mat. Res. Soc. Symp. Proc.*, **317**, 283(1994).

30. Kubo, M., Y. Oumi, R. Miura, A. Stirling, and A. Miyamoto, *Ceram. Proc.*, **43**, 11 A, 2765(1997).

APPENDIX
COMPUTER PROGRAM

```
%THIS PROGRAM SOLVES THE WILKINSON HYDRODYNAMIC FOR FILM
%THICKNESS
%THE FUNCTION DIPMDR CONTAINS THE DIFFERENTIAL EQUATIONS
% DEFINITON OF THE VARIABLES
%PL=PRECURSOR SOLUTION DENSITY  PTH=LAALO3 FILM DENSITY
%VIS=VISCOSITY OF PRECURSOR SOLTUON(PA.S) SURF= SURFACE
%TENSION OF SOLUTION(N/M)
%CA=CAPILLARY NUMBER TINF=DIMENSIONLESS EQUILIBRIUM COATING
%THICKNESS
%HINF=STEADY STATE LIQUID FILM THICKNESS(M)
%TFILM=DRIED FILM THICKNESS(ANGSTROM)
%XINF=TRANSITION DISTANCE FROM REGION 2 TO REGION 3
%VARLEN=LENGTH OF REGION IN WHICH COATING THICKNESS VARIES
%FILM COATING LENGTH IS ASSUMED TO BE 8MM
%Q,P,L ARE THE PARAMETERS THAT RESULT FROM CONVERTING THE 3RD
%ORDER DIFFERENTIAL EQUATION(MODEL)
%INTO 3 FIRST ORDER DIFFERENTIAL EQUATIONS. L=THICKNESS
%PARAMETER


%CALCULATION OF THE CONSTANTS REQUIRED FOR THE DIFFERENTIAL
%EQUATION----------

GLOBAL A B CA
HOLD OFF
PL=1541;
PTH=6000;
VIS=.0025;
V=3.1.*0.01./60;
SURF=.04;
CA=VIS.*V./SURF;
TINF=0.944*(CA).^(1/6);
HINF=TINF*(VIS.*V./(PL*9.8)).^0.5;
C=0.075;
TFILM=HINF*C*(PL/PTH)*1E10;
A=(3*CA).^(2/3).*(1-TINF.^2/3);
B=1-TINF.^2;
K=0.68*CA.^(-1/6)*TINF;
XINF=(2.*SURF/(1541*9.8)).^0.5*1000;
TR=HINF.*(3*CA).^(-1/3);
```

```
%--------------------------------INITIAL CONDITIONS-----------------------------------

Q=0;
P=0;
L=1.0001;
F=ZEROS(3,1);


%-----------------SOLUTION OF THE DIFFERENTIAL EQUATION--------------------

NQ=48;
TSPAN=ZEROS(2,1);
TSPAN=[0 NQ];
F=[Q P L]';
[TP YP]=ODE45('DIPMDR',TSPAN,F);
DIST=1000*(NQ-TP).*TR;
[M N]=SIZE(YP);
[MM NN]=MIN(ABS(YP(:,1)-K));
YY=1-TP./NQ;
LEN=YP(:,3)*TFILM
PERCENT=100*(1-NN/M)
VARLEN=XINF./(1-NN/M);
YAXIS=VARLEN*YY
RATIO=LEN(M)./LEN(1);

%--------------------------PLOTTING OF THE DATA---------------------------

PLOT(LEN,YAXIS)
TITLE('LIQUID FILM THICKNESS VS DISTANCE ALONG SAMPLE')
XLABEL('LIQUID FILM THICKNESS (ANGSTROM)')
YLABEL('DISTANCE ALONG SAMPLE(MM)')
HOLD ON
REG2=VARLEN*ONES(M,1);
REG3=XINF*ONES(M,1);

PLOT(LEN,REG2,'G')
HOLD ON

PLOT(LEN,REG3,'R')
HOLD ON

FOR I=1:100
  DISTINF(I)=8-(8-VARLEN)*I./100;
  YPINF(I)=TFILM;
```

```
  PLOT(YPINF(I),DISTINF(I),'B')
END
%THIS PROGRAM CALCULATES THE DERIVATIVES FOR THE MAIN
%PROGRAM
FUNCTION YPDOT=DIPMDR(TP,YP)
GLOBAL A B CA

YPDOT=ZEROS(3,1);
YPDOT(1)=A.*(YP(1)./YP(3).^2-2*YP(2)./YP(3).^3)-B.*(YP(3)-1)./YP(3).^3;
YPDOT(2)=YP(1);
YPDOT(3)=YP(2);
```

VITA

Vineet Kevin Lasrado was born in Bombay, India on September 14, 1974. He attended Our Lady of Perpetual Succour High School from June 1980 to March 1990 where he completed his high school education. Upon graduation from high school in March 1990, he joined Swami Vivekanada Junior College, where he completed two years of the higher secondary course in March 1992. He entered University of Bombay, Department of Chemical Technology at Bombay, in July 1992 and graduated with a Bachelor of Chemical Engineering, in May 1996. In August 1996, he entered the University of Tennessee Space Institute in the Department of Chemical Engineering. He received a Master of Science with a major in Chemical Engineering at UTSI in December 1998.